

ALP-mediated Dark Matter-Nucleon Scattering

Wim Beenakker,^{1,2} Daniël Mikkers,¹ Anh Vu Phan,^{1,2} Susanne Westhoff^{1,2}

¹*Institute for Mathematics, Astrophysics and Particle Physics, Radboud University, 6500 GL Nijmegen, The Netherlands*

²*Nikhef, Science Park 105, 1098 XG Amsterdam, The Netherlands*

E-mail: w.beenakker@science.ru.nl, danielmikkers@proton.me,
anhvu.phan@ru.nl, susanne.westhoff@ru.nl

ABSTRACT: We perform a comprehensive analysis of dark matter-nucleon scattering via the exchange of axion-like particles (ALPs). At first sight, this might appear of little practical use, as non-relativistic scattering through pseudo-scalar interactions is momentum-suppressed and spin-dependent, resulting in scattering rates below any experimental sensitivity. We show that the scattering rate can be drastically enhanced in two ways. First, light ALPs with masses below the typical momentum transfer at direct detection experiments lift the momentum suppression by acting as essentially massless mediators. Second, ALP exchange through loops induces coherent spin-independent scattering. If the ALP has flavor-changing couplings to up-type quarks, loop-induced scattering receives an extra strong enhancement by the top-quark mass. We deduce that, contrary to common lore, XENONnT and PandaX-4T are already sensitive to ALP-mediated dark matter-nucleon scattering. The next generation of direct detection experiments will probe far into the parameter space of the ALP effective theory, potentially exceeding the sensitivity of collider searches.

Contents

1	Introduction	1
2	ALP effective theory and dark matter	3
2.1	ALP couplings to Standard Model particles and fermion dark matter	3
2.2	Experimental bounds on ALP couplings to light quarks and gluons	5
2.3	Experimental bounds on flavor-changing ALP couplings	8
3	ALP-mediated dark matter-nucleus scattering	11
3.1	Heavy ALP mediator	12
3.2	Light ALP mediator	13
3.3	Non-relativistic scattering	16
3.4	Dark matter-nucleus scattering	16
4	Tree level: spin-dependent scattering	18
4.1	Heavy ALP mediator	18
4.2	Light ALP mediator	19
5	Loop level: spin-independent scattering	20
5.1	Flavor-diagonal ALP couplings	21
5.2	Flavor-changing ALP couplings	23
5.3	Pion loops in chiral perturbation theory	25
5.4	Higher-order ALP couplings	28
6	Numerical results	29
6.1	Flavor-diagonal ALP couplings	30
6.2	Flavor-changing ALP couplings	31
6.3	Predictions for Xenon-based experiments	32
7	Conclusion	36
A	Loop functions for spin-independent scattering	37

1 Introduction

Over the past years, dark matter direct detection experiments have reached a remarkable sensitivity to dark matter-nucleon scattering [1–3]. In many models for particle dark matter (DM), the null results of searches set the strongest constraints on the underlying fundamental interactions with quarks and gluons [4–6]. Classified by their Lorentz structure, scalar and vector interactions induce coherent spin-independent scattering. Pseudo-scalar

and axial-vector interactions lead to spin-dependent scattering, which is comparatively suppressed for heavy nuclei [7, 8]. In addition, pseudo-scalar interactions are momentum-suppressed in the non-relativistic regime probed by experiments. For Xenon nuclei, scattering through pseudo-scalar interactions is about 8 orders of magnitude smaller than scattering through scalar or vector interactions.

It seems a logical consequence that dark matter-nucleon scattering through pseudo-scalar mediators has been underexplored. Among the one-particle portals to a dark sector [9–11], Higgs-mixing scalars [12–14] and dark photons [15, 16] have been established as benchmark scenarios to compare the sensitivity of direct detection experiments among themselves and against other dark matter searches. On the contrary, axion-like particles (ALPs) as pseudo-scalar mediators of dark matter-nucleon scattering have received much less attention. This lack of exploration makes it difficult, if not impossible, to estimate the detection prospects of ALP-mediated dark matter and link the corresponding searches to other experimental probes.

In this work, we perform the first comprehensive analysis of dark matter-nucleon scattering through ALPs. We show that ALP-mediated scattering is actually observable at current direct detection experiments, provided that the ALP is light compared to the momentum exchange with nucleons or has flavor-changing couplings to top quarks.

Let us briefly review the state of the art in dark matter-nucleon scattering through pseudo-scalar mediators in general and ALPs in particular. Dark matter models which induce primarily spin-dependent interactions have been classified in [8]. For generic pseudo-scalars, it was found that the momentum suppression of spin-dependent scattering can be lifted by a light mediator [17] and that many models generate spin-independent scattering at the loop level [17–19]. The lifting of momentum suppression for light ALPs has also been investigated in dark matter-electron scattering [20].

If the pseudo-scalar mediator is an ALP, the phenomenology changes because ALP interactions respect a shift symmetry, which prevents fundamental couplings of ALPs with particles of the Standard Model (SM). ALP interactions are therefore described by an effective field theory (EFT) with a cutoff scale far above the momentum scale of dark matter-nucleon scattering [21]. As a consequence, the suppression of spin-dependent scattering at tree level over spin-independent scattering at loop level is reduced: The former is suppressed quadratically, the latter by four powers of the cutoff scale. This viewpoint is reflected in recent analyses of ALP-mediated dark matter, which claim dark matter-nucleon scattering to be suppressed below the reach of current experiments [22, 23]. As we will show, this conclusion is circumvented in the presence of flavor-changing ALP couplings, which raise spin-independent scattering to an observable level through a new enhancement mechanism.

ALPs are not only viable mediators of a dark force today, but also throughout the cosmic history. For fermion dark matter, the cosmologically relevant parameter space has been mapped out for generic ALP mediators with couplings to gluons [22] and leptons [23], and

for the QCD axion as a mediator [24]. It was found that the observed relic dark matter abundance can be obtained from various cosmic histories, including freeze-in and freeze-out scenarios. These cosmological benchmarks can give valuable hints for ALP-mediated dark matter searches at laboratory experiments.

Our analysis of ALP-mediated dark matter-nucleon scattering is organized as follows. In section 2, we review the ALP effective theory and derive experimental bounds on the relevant ALP couplings with quarks and gluons. In section 3, we discuss the formalism for non-relativistic dark matter-nucleus scattering through contact interactions and through light mediators within the ALP effective theory. Section 4 is devoted to spin-dependent scattering through heavy and light ALPs at tree level. In section 5, we calculate loop-induced spin-independent scattering for three separate contributions: flavor-diagonal ALP couplings in section 5.1, flavor-changing ALP couplings in section 5.2, and non-perturbative contributions from light meson exchange in chiral perturbation theory (chPT) in section 5.3. We also comment on potential contributions from higher-order couplings in the ALP effective theory in section 5.4. In section 6, we quantify all these individual contributions to ALP-mediated dark matter-nucleon scattering and provide numerical predictions of event rates at current and future direct detection experiments. We conclude in section 7. Technical details on the loop functions and the chiral Lagrangian are relegated to section A.

2 ALP effective theory and dark matter

In this section, we briefly review the effective theory of ALP interactions and introduce the relevant couplings to SM particles and dark matter. Throughout this work, we assume that dark matter consists of Dirac fermions. Other dark matter candidates are possible, but would lead to a different phenomenology of dark matter-nucleon scattering. They deserve a separate analysis.

ALP couplings are constrained by a number of searches at collider experiments and by astrophysical observables. For the relevant couplings in dark matter-nucleon scattering, we derive the current bounds from colliders over a broad range of ALP masses. Astrophysics typically provides stronger bounds than colliders on ALPs with masses below about 10 MeV, see e.g. [25–27]. At this mass scale, the ALP is essentially massless in dark matter-nucleon scattering at current experiments and the scattering phenomenology is similar to somewhat heavier ALPs, which do not leave a trace in astrophysics. We therefore do not consider astrophysical bounds in this work.

2.1 ALP couplings to Standard Model particles and fermion dark matter

The ALP effective theory includes all ALP interactions with SM particles that preserve a shift symmetry of the ALP field, $a \rightarrow a + c$, with c being a constant. We assume that this shift symmetry is also preserved by the ALP coupling to dark matter fermions. In this case, the effective Lagrangian for ALP interactions that are relevant for dark matter-

nucleon scattering reads [21, 28]

$$\begin{aligned}
\mathcal{L}_{\text{eff}}(\mu) = & \frac{1}{2} \partial_\mu a \partial^\mu a - \frac{m_a^2}{2} a^2 + i\bar{\chi}\gamma^\mu\partial_\mu\chi - m_\chi\bar{\chi}\chi + \frac{c_\chi}{2} \frac{\partial^\mu a}{f_a} \bar{\chi}\gamma_\mu\gamma_5\chi \\
& + \frac{\partial^\mu a}{f_a} \bar{U}_L \mathbf{c}_U \gamma_\mu U_L + \frac{\partial^\mu a}{f_a} \bar{D}_L \mathbf{c}_D \gamma_\mu D_L + \frac{\partial^\mu a}{f_a} \bar{U}_R \mathbf{c}_u \gamma_\mu U_R + \frac{\partial^\mu a}{f_a} \bar{D}_R \mathbf{c}_d \gamma_\mu D_R \\
& + c_{GG} \frac{a}{f_a} \frac{\alpha_s}{4\pi} G_{\mu\nu}^b \tilde{G}^{b,\mu\nu}.
\end{aligned} \tag{2.1}$$

Here a is the ALP field with associated mass m_a , and χ is a Dirac fermion without any charge under the SM gauge group. Further, $G_{\mu\nu}^b$ denotes the gluon field strength tensor and its dual is $\tilde{G}^{b,\mu\nu} = \frac{1}{2} \epsilon^{\mu\nu\rho\sigma} G_{\rho\sigma}^b$, with $SU(3)_C$ gauge indices $b = \{1, \dots, 8\}$ and the strong coupling α_s . The quark fields correspond to mass eigenstates; U, D are 3-vectors and \mathbf{c}_i are 3×3 matrices, both in flavor space. The ALP couplings to left-handed up- and down-type quarks are related by the CKM matrix V via $\mathbf{c}_D = V^\dagger \mathbf{c}_U V$. All parameters in this Lagrangian are defined at a scale $\mu < \Lambda = 4\pi f_a$ below the cutoff scale Λ . Throughout this work, we set $f_a = 1 \text{ TeV}$, reflecting the fact that so far no fundamental particles beyond the Standard Model have been observed below the TeV scale.

It is convenient to write the ALP couplings to up-type quarks in terms of axial-vector and vector parts,

$$\mathcal{L}_{\text{eff}} \supset \frac{\partial^\mu a}{2f_a} \bar{U} (\mathbf{c}_u - \mathbf{c}_U) \gamma_\mu \gamma_5 U + \frac{\partial^\mu a}{2f_a} \bar{U} (\mathbf{c}_u + \mathbf{c}_U) \gamma_\mu U, \tag{2.2}$$

and analogously for down-type quarks with $u \rightarrow d$ and $U \rightarrow D$. For on-shell quarks, applying integration by parts and the Dirac equation to (2.2) leads to

$$\mathcal{L}_{\text{eff}} \supset -\frac{ia}{2f_a} \sum_{i,j} [(m_{u_i} + m_{u_j}) \bar{U}_i (\mathbf{c}_u - \mathbf{c}_U)_{ij} \gamma_5 U_j + (m_{u_i} - m_{u_j}) \bar{U}_i (\mathbf{c}_u + \mathbf{c}_U)_{ij} U_j], \tag{2.3}$$

with the generation indices $i, j = \{1, 2, 3\}$. The flavor-diagonal (FD) ALP couplings to up-type quarks,

$$c_{uu} = (\mathbf{c}_u - \mathbf{c}_U)_{11}, \quad c_{cc} = (\mathbf{c}_u - \mathbf{c}_U)_{22}, \quad c_{tt} = (\mathbf{c}_u - \mathbf{c}_U)_{33}, \tag{2.4}$$

originate from the axial-vector current in (2.2). Analogous expressions hold for down-type quarks. The vector part $(\mathbf{c}_u + \mathbf{c}_U)_{ii}$ is unobservable in processes which preserve flavor-diagonal vector currents, including QED, QCD and dark-sector interactions. Flavor-changing (FC) couplings, in turn, receive both axial-vector and vector contributions. In this work, the relevant flavor-changing couplings are the up-top couplings

$$c_{ut}^A = (\mathbf{c}_u - \mathbf{c}_U)_{13}, \quad c_{ut}^V = (\mathbf{c}_u + \mathbf{c}_U)_{13} \tag{2.5}$$

and couplings in the down-quark sector

$$c_{d_i d_j}^A = (\mathbf{c}_d - \mathbf{c}_D)_{ij}, \quad c_{d_i d_j}^V = (\mathbf{c}_d + \mathbf{c}_D)_{ij}, \tag{2.6}$$

where the quark flavors are denoted as $d_1 = d, d_2 = s, d_3 = b$. Hermiticity of the Lagrangian requires $c_{ij}^{A,V} = (c_{ji}^{A,V})^*$.

2.2 Experimental bounds on ALP couplings to light quarks and gluons

The couplings of ALPs to particles of the Standard Model are experimentally constrained by a large number of measurements and searches at particle physics experiments. For this work, ALP couplings to quarks and gluons are most relevant. In this section, we summarize existing bounds on the ALP-gluon coupling and on flavor-diagonal ALP couplings to up and down quarks.

When deriving bounds on the various ALP couplings, we assume that only the considered coupling is present at the cutoff scale Λ . Additional couplings can change the derived bounds in the observables we consider and make other observables sensitive to the coupling of interest.

The ALP coupling to dark matter is not constrained independently of the ALP-SM couplings by collider searches. We therefore apply only the loose perturbativity bound $c_\chi < 4\pi$. We also neglect potential ALP decays to dark matter, $a \rightarrow \chi\bar{\chi}$. If present, they would strengthen the bounds on other ALP couplings from searches for $K \rightarrow \pi a$ and $B \rightarrow (K, \pi) a$ decays with invisible ALPs.

ALP decays ALPs with couplings to gluons and quarks of the first generation decay mostly hadronically, provided that the ALP mass lies above the three-pion threshold, $m_a > 3m_\pi$. For ALP masses in the perturbative regime, $m_a \gg 2 \text{ GeV}$, the decay width for ALPs into light-flavored hadrons is given by [29, 30]

$$\Gamma(a \rightarrow \text{hadrons}) \approx \frac{|C_{GG}^{\text{eff}}(m_a)|^2}{23 \text{ nm}} \left(\frac{\alpha_s(m_a)}{0.3} \right)^2 \left(\frac{m_a}{2 \text{ GeV}} \right)^3 \left(\frac{1 \text{ TeV}}{f_a} \right)^2. \quad (2.7)$$

We quote the decay width in units of inverse length to give an impression of the corresponding proper decay length. For $m_a \ll m_t$, the effective ALP-gluon coupling can be expressed in terms of the couplings at the cutoff scale as

$$C_{GG}^{\text{eff}}(m_a) \approx 0.96 c_{GG} + 0.48 [c_{uu}(\Lambda) + c_{dd}(\Lambda)]. \quad (2.8)$$

For ALP masses $3m_\pi < m_a < 2 \text{ GeV}$, the decay channels $a \rightarrow 3\pi = \{3\pi^0, \pi^+\pi^-\pi^0\}$ dominate. Away from the kinematic threshold, $m_a \gg 3m_\pi$, the decay width for the sum of both final states is¹

$$\Gamma(a \rightarrow 3\pi) \approx \frac{[0.73 c_{GG} + c_{uu}(\Lambda) - c_{dd}(\Lambda)]^2}{1 \text{ mm}} \left(\frac{m_a}{1 \text{ GeV}} \right)^3 \left(\frac{1 \text{ TeV}}{f_a} \right)^2. \quad (2.9)$$

ALPs with masses below the hadronic threshold, $m_a < 3m_\pi$, decay mostly into two photons through renormalization group (RG) effects of ALP-gluon and ALP-quark couplings present at the cutoff scale. The decay width is given by [30]

$$\Gamma(a \rightarrow \gamma\gamma) = \frac{\alpha^2}{64\pi^3} \frac{m_a^3}{f_a^2} |C_{\gamma\gamma}^{\text{eff}}(m_a)|^2 = \frac{|C_{\gamma\gamma}^{\text{eff}}(m_a)|^2}{7 \text{ mm}} \left(\frac{m_a}{1 \text{ GeV}} \right)^3 \left(\frac{1 \text{ TeV}}{f_a} \right)^2, \quad (2.10)$$

¹The decay width including the full phase-space dependence can be found in [30].

valid for any ALP mass. For ALPs with masses in the perturbative regime of QCD, the effective ALP-photon coupling is [28, 30]

$$C_{\gamma\gamma}^{\text{eff}}(m_a \gg 2 \text{ GeV}) \approx -0.12 c_{GG} + 1.27 c_{uu}(\Lambda) + 0.27 c_{dd}(\Lambda). \quad (2.11)$$

Below the scale of chiral symmetry breaking, $\mu_{\text{chPT}} \approx 2 \text{ GeV}$, additional non-perturbative contributions result in [28, 30]

$$C_{\gamma\gamma}^{\text{eff}}(m_a < \mu_{\text{chPT}}) \approx - \left(1.92 + 0.36 \frac{m_a^2}{m_\pi^2 - m_a^2} \right) c_{GG} - \frac{1}{2} \frac{m_a^2}{m_\pi^2 - m_a^2} [c_{uu}(\Lambda) - c_{dd}(\Lambda)]. \quad (2.12)$$

Depending on the ALP properties and the setup of the experiment, the ALP might decay mostly outside the detector and appear as invisible.

ALP production in meson decays Light ALPs can be produced in the meson decays $K \rightarrow \pi a$ and $B \rightarrow Ka$ through the flavor-changing neutral currents c_{ds}^V and c_{sb}^V , defined in eq. (2.6). We assume that $c_{d_i d_j}^A(\Lambda) = c_{d_i d_j}^V(\Lambda) = 0$ for $i \neq j$, which implies $\mathbf{c}_U = 0$. In this case, the meson decays are loop-induced, which leads to the smallest decay widths and most conservative bounds on the ALP couplings c_{GG} , c_{uu} and c_{dd} . For kaon decays, the branching ratio into ALPs has been calculated in chPT [30], yielding

$$\mathcal{B}(K^- \rightarrow \pi^- a) \approx 7 \cdot 10^{-7} \frac{[c_{GG} + 0.5 c_{uu}(\Lambda) + 0.2 c_{dd}(\Lambda)]^2}{(f_a/1 \text{ TeV})^2} \lambda^{1/2} \left(\frac{m_\pi^2}{m_K^2}, \frac{m_a^2}{m_K^2} \right), \quad (2.13)$$

with $\lambda(x, y) = 1 + x^2 + y^2 - 2(x + y + xy)$. For B decays, the branching ratio into ALPs can be calculated in perturbation theory, see e.g. [31]), which yields

$$\mathcal{B}(B^- \rightarrow K^- a) \approx 4.6 \cdot 10^{-6} \frac{[c_{GG} + 0.5 c_{uu}(\Lambda) + 0.5 c_{dd}(\Lambda)]^2}{(f_a/1 \text{ TeV})^2} \frac{f_0^2(m_a^2)}{f_0^2(0)} \lambda^{1/2} \left(\frac{m_K^2}{m_B^2}, \frac{m_a^2}{m_B^2} \right). \quad (2.14)$$

Here we have used the scalar hadronic form factor $f_0(0)$ from [32].

ALP couplings to gluons At the NA62 experiment, ALPs can be produced from kaon decays $K \rightarrow \pi a$. In this mass region, hadronic decays such as $a \rightarrow 3\pi$ are kinematically forbidden and the dominant decay mode is $a \rightarrow \gamma\gamma$. For ALPs with masses $m_a \lesssim 0.126 c_{GG}^{-2/3} \text{ GeV}$, assuming $f_a = 1 \text{ TeV}$, the proper lifetime exceeds 5 ns, except for ALP masses close to the pion mass. For $m_a < m_K - m_\pi$, this condition is fulfilled for $c_{GG} < 0.2$. In this case, the produced ALPs decay mostly outside the NA62 detector and the search for $K^+ \rightarrow \pi^+ X$ with an invisible particle X [33] applies. The sensitivity of this search to the ALP-gluon coupling depends on the ALP mass. For $m_a > m_\pi$, NA62 finds an upper bound of $\mathcal{B}(K^+ \rightarrow \pi^+ X) \lesssim 10^{-11}$, which corresponds to

$$m_\pi < m_a < m_K - m_\pi : \quad \frac{|c_{GG}|}{f_a} \lesssim \frac{0.0038}{\text{TeV}}. \quad (2.15)$$

For $m_a < m_\pi$, the bound on the branching ratio is a factor of 2–3 weaker. Notice that the search excludes the mass region of strong ALP-pion mixing, $m_a \approx m_\pi$, which is constrained by a separate search for $K^+ \rightarrow \pi^+\pi^0, \pi^0 \rightarrow \textit{invisible}$ by NA62 [34].

For couplings $c_{GG} > 0.2$, the ALP decay length is reduced and the search loses sensitivity. In this parameter region, searches for $K_L \rightarrow \pi^0\nu\bar{\nu}$ [30] and $B^+ \rightarrow K^+\nu\bar{\nu}$ [31, 35] exclude all of the ALP parameter space for $m_a < 100$ MeV. Heavier ALPs with strong gluon couplings are constrained by searches for di-muon and di-photon final states [30]. The strongest bound in this mass region is due to a search for $B^\pm \rightarrow K^\pm a, a \rightarrow \gamma\gamma$ with proper decay length $c\tau_a \lesssim 1$ mm at the BaBar experiment [36], which imposes

$$0.175 \text{ GeV} < m_a \lesssim 2 \text{ GeV} : \quad \frac{|c_{GG}|}{f_a} \lesssim \frac{0.23}{\text{TeV}}. \quad (2.16)$$

For ALPs with masses $m_a \gtrsim 2$ GeV, the branching fraction into di-photons is strongly suppressed due to the overwhelming decay into light-flavored hadrons.

For ALPs too heavy to be resonantly produced in meson decays, dijet production at the LHC offers a direct probe of the ALP-gluon coupling. In particular, angular correlations in dijet distributions are modified by the exchange of a virtual ALP, leading to the loose bound [37, 38]

$$m_a \ll M_{jj} : \quad \frac{|c_{GG}|}{f_a} \lesssim \frac{100}{\text{TeV}}. \quad (2.17)$$

For ALP masses well below the dijet invariant mass, M_{jj} , this bound is largely independent of the ALP mass.

Flavor-diagonal ALP couplings to up and down quarks As described above, ALPs with couplings to up and down quarks have a similar phenomenology as ALPs with gluon couplings. With pure ALP couplings to light quarks, ALPs below the hadronic threshold decay dominantly via $a \rightarrow \gamma\gamma$, with a proper lifetime of $\tau_a \gtrsim 5$ ns for $m_a \lesssim 0.270 |c_{uu}(\Lambda) - c_{dd}(\Lambda)|^{-2/3}$ GeV, assuming $f_a = 1$ TeV. Using NA62’s search for $K^+ \rightarrow \pi^+ X$ again [33], we obtain

$$m_\pi < m_a < m_K - m_\pi : \quad \frac{|c_{uu}(\Lambda) + 0.4 c_{dd}(\Lambda)|}{f_a} \lesssim \frac{0.0076}{\text{TeV}}, \quad (2.18)$$

and somewhat looser bounds for ALP masses below the pion mass. These bounds apply for ALP couplings $|c_{uu}(\Lambda) - c_{dd}(\Lambda)| < 0.67$, due to the lifetime sensitivity. The parameter space of larger couplings is excluded by searches for $K_L \rightarrow \pi^0\nu\bar{\nu}$ and $B^+ \rightarrow K^+\nu\bar{\nu}$, as for ALP-gluon couplings.

For ALPs heavier than kaons, hadronic decays dominate and the ALP is short-lived at detector scales. The currently strongest bound is due to the same BaBar search for $B^+ \rightarrow K^+ a, a \rightarrow \gamma\gamma$ mentioned earlier [36], yielding

$$0.175 \text{ GeV} < m_a \lesssim 2 \text{ GeV} : \quad \frac{|c_{uu}(\Lambda) + c_{dd}(\Lambda)|}{f_a} \lesssim \frac{1.6}{\text{TeV}}. \quad (2.19)$$

For ALPs with $m_a \gtrsim 2 \text{ GeV}$, predictions of ALP decays are challenged by the presence of hadronic resonances. We therefore do not attempt to derive a bound from $B \rightarrow Ka, a \rightarrow \gamma\gamma$ in this region. In the perturbative QCD regime with $m_a \gg 2 \text{ GeV}$, ALP couplings to light quarks are strongly suppressed with the quark mass. Collider searches therefore do not impose any bounds on c_{uu} and c_{dd} in this mass region.

2.3 Experimental bounds on flavor-changing ALP couplings

In ALP-mediated dark matter-nucleon scattering, the flavor-changing ALP couplings $c_{ut}^{V,A}$ from eq. (2.5) play a special role for reasons that will become clear later. In this section, we derive bounds on $c_{ut}^{V,A}$ from collider searches for ALPs in a broad range of masses. As before, we assume that only this coupling is present at the cutoff scale of the ALP effective theory, and we neglect ALP decays to dark matter.

ALP decays ALPs with masses larger than the top mass, $m_a > m_t$, decay mostly through $a \rightarrow t\bar{u}$. For real couplings $c_{ut}^{V,A}$, the corresponding decay width reads

$$\Gamma_{a \rightarrow t\bar{u}} = \Gamma_{a \rightarrow \bar{t}u} = \frac{3m_a}{32\pi} [(c_{ut}^V)^2 + (c_{ut}^A)^2] \frac{m_t^2}{f_a^2} \left(1 - \frac{m_t^2}{m_a^2}\right)^2. \quad (2.20)$$

Such heavy ALPs decay promptly within the detector, unless the couplings are strongly suppressed.

Through the CKM relation $\mathbf{c}_D = V^\dagger \mathbf{c}_U V$, the ALP couplings $c_{ut}^{V,A}$ induce flavor-changing down-quark couplings at tree level [28, 39],

$$(\mathbf{c}_D)_{ij} = \frac{1}{2} [V_{1i}^*(c_{ut}^V - c_{ut}^A)V_{3j} + V_{3i}^*(c_{tu}^V - c_{tu}^A)V_{1j}] \stackrel{\text{real}}{=} \frac{1}{2} (c_{ut}^V - c_{ut}^A)(V_{1i}^*V_{3j} + V_{3i}^*V_{1j}). \quad (2.21)$$

Throughout our analysis, we will assume real ALP couplings $c_{ut}^{V,A}$, so that the last relation applies. These couplings induce hadronic ALP decays, which dominate for $m_a < m_t$ wherever kinematically allowed.

For ALPs with masses $\mu_{\text{chPT}} < m_a < m_t$, these hadronic decays can be calculated perturbatively. In the limit $m_a \gg m_{d_i}, m_{d_j}$, the partial decay width reads

$$\Gamma_{a \rightarrow d_i \bar{d}_j} = \frac{3m_a}{16\pi} |(\mathbf{c}_D)_{ij}|^2 \frac{m_{d_i}^2 + m_{d_j}^2}{f_a^2}. \quad (2.22)$$

Due to the CKM structure of the coupling and the quark mass dependence of the decay rate, the ALP decays dominantly into a $b\bar{d}$ or $\bar{b}d$ pair, if kinematically allowed. The corresponding decay length is

$$\lambda_a \approx \frac{26.4 \text{ pm}}{|c_{ut}^V - c_{ut}^A|^2} \frac{10 \text{ GeV}}{m_a} \left(\frac{5 \text{ GeV}}{m_b}\right)^2 \left(\frac{f_a}{1 \text{ TeV}}\right)^2. \quad (2.23)$$

ALPs with $m_a > m_B$ decay promptly at colliders, unless $c_{ut}^V \approx c_{ut}^A$. This case, however, is not relevant for this work, since ALP-induced dark matter-nucleon scattering vanishes for $|c_{ut}^V| = |c_{ut}^A|$.

For ALPs with masses $m_a < \mu_{\text{chPT}}$, hadronic interactions with mesons can be described in chiral perturbation theory (chPT). Focusing on \mathbf{c}_D -induced interactions, the chiral Lagrangian reads [30]

$$\mathcal{L}_{\text{chPT}} \supset \frac{f_\pi^2}{8} \text{Tr} \left[(\mathbf{D}^\mu \boldsymbol{\Sigma})(\mathbf{D}_\mu \boldsymbol{\Sigma})^\dagger \right] + \frac{f_\pi^2}{4} B_0 \text{Tr} \left[\mathbf{m}_q (\boldsymbol{\Sigma}^\dagger + \boldsymbol{\Sigma}) \right], \quad (2.24)$$

with the pion decay constant $f_\pi \approx 130.5 \text{ MeV}$, the diagonal 3×3 quark-mass matrix \mathbf{m}_q , the chPT parameters $B_0 m_u = (6.2 \pm 0.4) \cdot 10^{-3} \text{ GeV}^2$, $B_0 m_d \approx (13.3 \pm 0.4) \cdot 10^{-3} \text{ GeV}^2$ [40], and the covariant derivative of the chiral multiplet

$$\mathbf{D}_\mu \boldsymbol{\Sigma} = \partial_\mu \boldsymbol{\Sigma} - i \frac{\partial_\mu a}{f_a} \mathbf{k}_D \boldsymbol{\Sigma}, \quad (2.25)$$

where

$$\boldsymbol{\Sigma} = \exp \left[\frac{2i}{f_\pi} \begin{pmatrix} \frac{\pi^0}{\sqrt{2}} + \frac{\eta_8}{\sqrt{6}} & \pi^+ & K^+ \\ \pi^- & -\frac{\pi^0}{\sqrt{2}} + \frac{\eta_8}{\sqrt{6}} & K^0 \\ K^- & \bar{K}^0 & -\frac{2\eta_8}{\sqrt{6}} \end{pmatrix} \right], \quad \mathbf{k}_D = \begin{pmatrix} 0 & 0 & 0 \\ 0 & 0 & (\mathbf{c}_D)_{12} \\ 0 & (\mathbf{c}_D)_{21} & 0 \end{pmatrix}. \quad (2.26)$$

Here the couplings $(\mathbf{c}_D)_{12}$ and $(\mathbf{c}_D)_{21}$ are evaluated at the electroweak scale $\mu_W \approx m_t$. Assuming real ALP couplings and expanding eq. (2.24) to first order in the ALP couplings and ALP interactions with up to two meson fields, we obtain

$$\begin{aligned} \mathcal{L}_{\text{chPT}} \supset & -\frac{f_\pi}{\sqrt{2} f_a} (\mathbf{c}_D)_{12} \partial^\mu a \partial_\mu K_L^0 \\ & + \frac{i}{2} \frac{(\mathbf{c}_D)_{12}}{f_a} a \left[K_S^0 \partial^2 (\pi^0 - \sqrt{3} \eta_8) - (\pi^0 - \sqrt{3} \eta_8) \partial^2 K_S^0 \right] \\ & + \frac{i}{2} \frac{(\mathbf{c}_D)_{12}}{f_a} a \left[K^- \partial^2 \pi^+ - \pi^+ \partial^2 K^- \right] + h.c., \end{aligned} \quad (2.27)$$

with $K_L^0 = (K^0 + \bar{K}^0)/\sqrt{2}$ and $K_S^0 = (K^0 - \bar{K}^0)/\sqrt{2}$. The first term induces kinetic mixing between the ALP and K_L^0 , through which the ALP can decay into three pions.² The terms in the second and third lines induce two-body decays of the ALP into light mesons. In particular, the decay width for $a \rightarrow K\pi$ is given by

$$\Gamma(a \rightarrow K\pi) = \frac{m_a}{64\pi} |(\mathbf{c}_D)_{12}|^2 \frac{(m_K^2 - m_\pi^2)^2}{f_a^2 m_a^2} \lambda^{1/2} \left(\frac{m_\pi^2}{m_a^2}, \frac{m_K^2}{m_a^2} \right). \quad (2.28)$$

Summing up the three channels $K_S^0 \pi^0$, $K^+ \pi^-$, $K^- \pi^+$ and neglecting mass differences, the decay length reads

$$\lambda_a \approx \frac{0.6 \text{ mm}}{|c_{ut}^V - c_{ut}^A|^2} \left(\frac{f_a}{1 \text{ TeV}} \right)^2 \left(\frac{m_a}{1 \text{ GeV}} \right) \lambda^{-1/2} \left(\frac{m_\pi^2}{m_a^2}, \frac{m_K^2}{m_a^2} \right). \quad (2.29)$$

To the best of our knowledge, this is the first time hadronic ALP decays through FC up-quark couplings are being investigated.

²Mass mixing between the ALP and the pseudo-scalar mesons is absent as long as $c_{GG} = 0$.

For ALPs with masses below the hadronic threshold, $m_\pi + m_e < m_a < 3m_\pi$, semileptonic decay $a \rightarrow \pi l \nu_l$, where $l = e, \mu$, is possible through kinetic mixing with K_L^0 . For even lighter ALPs, decay into two photons is possible, but two-loop-suppressed. In both cases, the ALP is long-lived and can be considered as detector-stable.

ALP production and bounds Heavy ALPs with masses up to the TeV scale can be produced at the LHC in association with a top quark. For $m_a > m_t$, the dominant production channel is through the single-top process $pp \rightarrow tja$, where j is a hadronic jet. For $m_a < m_t$, the ALP can also be produced from top decays in $pp \rightarrow t\bar{t} \rightarrow tja$. Both processes result in the same final-state particles, but with different kinematics. Depending on whether the ALP decays hadronically or invisibly, the signature consists of a reconstructed top quark and multiple jets or missing energy. In [41, 42], such signatures have been investigated for long-lived ALPs. The resulting bound of

$$\frac{|(\mathbf{c}_u)_{13}|}{f_a} = \frac{|c_{ut}^V + c_{ut}^A|}{2f_a} \lesssim \frac{0.1}{\text{TeV}} \quad (2.30)$$

applies if the ALP has only couplings to right-handed up-type quarks and no flavor-diagonal couplings to quarks.

ALPs with a coupling to left-handed quarks $(\mathbf{c}_U)_{13} = (c_{ut}^V - c_{ut}^A)/2$ decay promptly through the induced down-quark couplings $(\mathbf{c}_D)_{ij}$ from eq. (2.21). In this case, measurements of top-quark kinematics can provide bounds on the ALP coupling, provided that the deviation from the Standard Model is moderate. In [43, 44], kinematic distortions in top-antitop production have been investigated for ALPs with a flavor-diagonal coupling c_{tt} , yielding $|c_{tt}|/f_a \lesssim 10/\text{TeV}$. We expect a similar sensitivity to $(\mathbf{c}_U)_{13}$ from kinematic distortions. Other high-energy observables like the top-quark width or loop-induced ALP production from Higgs decays lead to even weaker bounds on c_{ut}^V and c_{ut}^A [28, 41]. A dedicated search for $pp \rightarrow tja$ with hadronic ALP decays, for instance via $a \rightarrow b\bar{d}, \bar{b}d$ with bottom jets in the final state, could enhance the sensitivity to $(\mathbf{c}_U)_{13}$.

Similar to flavor-diagonal couplings, ALPs with masses $m_a \lesssim 5 \text{ GeV}$ can be produced in meson decays $B \rightarrow Ka$, $B \rightarrow \pi a$ or $K \rightarrow \pi a$, if kinematically accessible. However, as $c_{ut}^V - c_{ut}^A$ induces flavor-changing down-quark couplings at tree level, ALPs with FC couplings can therefore be produced at high rates in meson decays. The branching ratios for $B^- \rightarrow K^- a$ and $B^- \rightarrow \pi^- a$ are [30, 31]

$$\begin{aligned} \mathcal{B}(B^- \rightarrow K^- a) &\approx 2.6 \cdot 10^3 |c_{ut}^V - c_{ut}^A|^2 \left(\frac{1 \text{ TeV}}{f_a}\right)^2 \frac{f_0^2(m_a^2)}{f_0^2(0)} \lambda^{1/2} \left(\frac{m_K^2}{m_B^2}, \frac{m_a^2}{m_B^2}\right), \\ \mathcal{B}(B^- \rightarrow \pi^- a) &\approx 6.5 \cdot 10^4 |c_{ut}^V - c_{ut}^A|^2 \left(\frac{1 \text{ TeV}}{f_a}\right)^2 \frac{f_{0,B \rightarrow \pi}^2(m_a^2)}{f_{0,B \rightarrow \pi}^2(0)} \lambda^{1/2} \left(\frac{m_\pi^2}{m_B^2}, \frac{m_a^2}{m_B^2}\right), \end{aligned} \quad (2.31)$$

where we have used the scalar hadronic form factors $f_0(q^2)$ [32] and $f_{0,B \rightarrow \pi}(q^2)$ [45]. To obtain these branching ratios, we have normalized the partial decay widths to the measured B meson width, Γ_B^{exp} [46].³ Notice that the branching ratio for $B \rightarrow \pi a$ is larger than for

³Numerically the branching ratios are much larger than those in [30, 31], as with FC ALP couplings the decay is induced at tree level, while FD couplings induce $B \rightarrow K$ and $B \rightarrow \pi$ through electroweak loops.

$B \rightarrow Ka$, due to the CKM structure of the induced down-quark couplings, see eq. (2.21). To probe $c_{ut}^{V,A}$, it can therefore be beneficial to explore $B \rightarrow \pi$ transitions in addition to the widely studied $B \rightarrow K$ transitions.

The most inclusive bound is obtained from the total width of the B meson. Demanding that $\mathcal{B}(B^- \rightarrow \pi^- a) < 1$, we obtain the bound

$$m_a < m_B - m_\pi : \quad \frac{|c_{ut}^V - c_{ut}^A|}{f_a} \lesssim \frac{0.004}{\text{TeV}}. \quad (2.32)$$

For couplings $|c_{ut}^V - c_{ut}^A|/f_a \lesssim (0.024/\text{TeV})(m_a/\text{GeV})^{1/2}$, the proper decay length of the ALP exceeds $c\tau_a = 1$ m and the ALP can be considered as long-lived at the Belle II experiment. In this case, Belle II's search for $B \rightarrow K\nu\bar{\nu}$ can be re-interpreted for an invisible intermediate ALP resonance. The latest re-interpretation has resulted in the bound $|(\mathbf{c}_D)_{23}|/f_a \lesssim (0.2 \dots 2) \cdot 10^{-5}/\text{TeV}$ [35], depending on the ALP mass, which translates to

$$m_a < m_B - m_K : \quad \frac{|c_{ut}^V - c_{ut}^A|}{f_a} \lesssim \frac{(0.18 \dots 1.8) \cdot 10^{-4}}{\text{TeV}}. \quad (2.33)$$

Taken together, the measurement of the total B meson width and the search for $B \rightarrow K\nu\bar{\nu}$ exclude the full range of coupling strength down to the bound of eq. (2.33).

For ALP masses $m_a < m_K - m_\pi$, fully hadronic decays are forbidden. Through kinetic mixing in chiral perturbation theory (2.27), the ALP inherits the decay modes of the K_L^0 , quadratically suppressed by the mixing parameter as $(f_\pi/f_a)^2$. Other possible decay modes are two-loop-suppressed. Due to the resulting long lifetime, the ALP can be considered as stable at fixed-target experiments and NA62's search for $K^+ \rightarrow \pi^+ X$ strikes again [33]. Using the partial decay rate for $K \rightarrow \pi a$ from [30] and the FC ALP coupling from eq. (2.21), we derive the bound

$$m_a < m_K - m_\pi : \quad \frac{|c_{ut}^V - c_{ut}^A|}{f_a} \lesssim \frac{(4.9 \dots 15.5) \cdot 10^{-8}}{\text{TeV}}, \quad (2.34)$$

which applies for ALP masses away from the pion mass.

3 ALP-mediated dark matter-nucleus scattering

At direct detection experiments, the typical momentum exchange in dark matter-nucleus scattering, $|\mathbf{q}| \lesssim 200$ MeV, is small compared to the mass of the nucleus and the dark matter particles in the experimentally accessible range. Dark matter-nucleus interactions are therefore conveniently described within an EFT framework. We start with the Lagrangian for the ALP effective theory (2.1) at the cutoff scale Λ , evolve the theory down to the scale of chiral symmetry breaking, $\mu_{\text{chPT}} \sim 2$ GeV, where we match it onto the chiral effective theory that describes non-perturbative dark matter-nucleon scattering via ALP exchange. As the ALP must be integrated out of the theory around its mass scale, we present this procedure separately for ALPs with mass $m_a > \mu_{\text{chPT}}$ (Section 3.1) and ALPs with $m_a < \mu_{\text{chPT}}$ (Section 3.2). In the non-relativistic regime at $|\mathbf{q}| \ll \mu_{\text{chPT}}$, the dark matter-nucleon interactions are finally matched onto dark matter-nucleus interactions using nuclear response functions. This last step is applicable to both heavy and light ALPs.

3.1 Heavy ALP mediator

To describe dark matter-nucleon interactions through heavy ALPs, we largely follow the formalism and notation from [40, 47]. If $m_a \gg \mu_{\text{chPT}}$, the ALP can be integrated out before matching onto the chiral Lagrangian. In this case, the ALP couplings from (2.1) induce dark matter interactions with quarks and gluons, which are described by an effective Lagrangian [47, 48]⁴

$$\mathcal{L}_{\chi q}(\mu_{\text{chPT}} < \mu < m_a) = C_G O_G + C_{\tilde{G}} O_{\tilde{G}} + \sum_{q=u,d,s} (C_S^q O_S^q + C_P^q O_P^q) + \dots \quad (3.1)$$

with the operators

$$\begin{aligned} O_G &= \frac{\alpha_s}{12\pi} (\bar{\chi}\chi) G^{b,\mu\nu} G_{\mu\nu}^b, \\ O_{\tilde{G}} &= \frac{\alpha_s}{8\pi} (\bar{\chi}i\gamma_5\chi) G^{b,\mu\nu} \tilde{G}_{\mu\nu}^b, \\ O_S^q &= m_q (\bar{\chi}\chi) (\bar{q}q), \\ O_P^q &= m_q (\bar{\chi}i\gamma_5\chi) (\bar{q}i\gamma_5q). \end{aligned} \quad (3.2)$$

To one-loop order in QCD, the Wilson coefficients $C_G, C_{\tilde{G}}, C_S^q$, and C_P^q are scale-independent, except for a threshold correction to C_G and $C_{\tilde{G}}$ each time a quark Q is integrated out at the scale $\mu_Q \approx m_Q$ [49]

$$\begin{aligned} C_G^{n_f}(\mu_Q) &= C_G^{n_f+1}(\mu_Q) - C_S^{Q,n_f+1}(\mu_Q), \\ C_{\tilde{G}}^{n_f}(\mu_Q) &= C_{\tilde{G}}^{n_f+1}(\mu_Q) + C_P^{Q,n_f+1}(\mu_Q). \end{aligned} \quad (3.3)$$

The superscript n_f denotes the number of active quark flavors in the effective theory; it will be suppressed in what follows. At the scale of chiral symmetry breaking, the Wilson coefficients can be directly expressed in terms of high-scale Wilson coefficients, yielding

$$\begin{aligned} C_S^{u,d,s}(\mu_{\text{chPT}}) &= C_S^{u,d,s}(m_a), \\ C_P^{u,d,s}(\mu_{\text{chPT}}) &= C_P^{u,d,s}(m_a), \\ C_G(\mu_{\text{chPT}}) &= C_G(m_a) - \sum_Q C_S^Q(m_a), \\ C_{\tilde{G}}(\mu_{\text{chPT}}) &= C_{\tilde{G}}(m_a) + \sum_Q C_P^Q(m_a). \end{aligned} \quad (3.4)$$

The sum over Q includes all quarks with $\mu_{\text{chPT}} < m_Q < m_a$.

At energies below $\mu_{\text{chPT}} \sim 2 \text{ GeV}$, quarks and gluons are confined inside color-neutral hadrons. The effective Lagrangian for (relativistic) dark matter interactions with nucleons $N = p, n$ reads

$$\mathcal{L}_{\chi N}(\mu < \mu_{\text{chPT}}) = \sum_{N=p,n} (C_S^N O_S^N + C_P^N O_P^N) + \dots, \quad (3.5)$$

⁴Here and in what follows, the dots represent terms that do not contribute to ALP-mediated dark matter-nucleon scattering at the lowest order.

with the operators for scalar and pseudo-scalar interactions,

$$\begin{aligned} O_S^N &= (\bar{\chi}\chi)(\bar{N}N), \\ O_P^N &= (\bar{\chi}i\gamma_5\chi)(\bar{N}i\gamma_5N). \end{aligned} \quad (3.6)$$

The DM-quark and DM-gluon Wilson coefficients from (3.4) match to the effective DM-nucleon interactions in chPT from (3.5) at tree level, which yields [40, 47]

$$\begin{aligned} C_S^N(q^2) &= C_G F_G^N(q^2) + \sum_{q=u,d,s} C_S^q F_S^{q/N}(q^2), \\ C_P^N(q^2) &= C_{\tilde{G}} F_{\tilde{G}}^N(q^2) + \sum_{q=u,d,s} C_P^q F_P^{q/N}(q^2). \end{aligned} \quad (3.7)$$

Here and throughout, $q^\mu = (E_R, \mathbf{q})$ is the four-momentum exchanged between the dark matter particle χ and the nucleon N , with recoil energy E_R and three-momentum \mathbf{q} . We define $\mathbf{q} = \mathbf{k}' - \mathbf{k}$, where \mathbf{k} and \mathbf{k}' are the three-momenta of the incoming and outgoing nucleon. The nucleon form factors $F_S^{q/N}, F_P^{q/N}, F_G^N, F_{\tilde{G}}^N$ describe the quark and gluon distributions inside the nucleons. They are defined as [47]

$$\begin{aligned} \langle N' | m_q \bar{q}q | N \rangle &= F_S^{q/N}(q^2) \bar{u}_{N'} u_N, \\ \langle N' | m_q \bar{q}i\gamma_5 q | N \rangle &= F_P^{q/N}(q^2) \bar{u}_{N'} i\gamma_5 u_N, \\ \langle N' | \frac{\alpha_s}{12\pi} G^{b\mu\nu} G_{\mu\nu}^b | N \rangle &= F_G^N(q^2) \bar{u}_{N'} u_N, \\ \langle N' | \frac{\alpha_s}{8\pi} G^{b\mu\nu} \tilde{G}_{\mu\nu}^b | N \rangle &= F_{\tilde{G}}^N(q^2) \bar{u}_{N'} i\gamma_5 u_N, \end{aligned} \quad (3.8)$$

where the nucleons are described by Dirac spinors $u_N, u_{N'}$ and N, N' refer to the same nucleon, but with different momentum. It is important to note that the matching in (3.7) only applies for DM-quark *contact* interactions, *i.e.*, for ALP masses $m_a \gg \mu_{\text{chPT}}$.

3.2 Light ALP mediator

If the ALP mass lies below or around the scale of chiral symmetry breaking, $m_a \lesssim \mu_{\text{chPT}}$, the ALP must be included as a particle in the chiral effective theory. Unlike in the case of a heavy ALP, dark matter-nucleon scattering through light ALPs cannot be described by a contact interaction and the procedure to calculate dark matter-nucleon interactions from section 3.1 cannot be used. Instead, one must evolve and match the ALP effective theory from (2.1) to the chiral effective theory of ALP-nucleon interactions and compute the dark matter-nucleon scattering in the presence of light ALPs. To our knowledge, dark matter-nucleon interactions through a light ALP have not been described in the literature, though they are mentioned in [22].

The chiral effective theory for ALP-nucleon interactions has originally been constructed in [21]. We follow the notation of [30]. Since the ALP has the same quantum numbers as the neutral pion, ALP-pion mixing plays a crucial role in determining the amplitude for dark matter-nucleon scattering.

Below the scale of chiral symmetry breaking, $\mu < \mu_{\text{chPT}}$, ALP-pion mixing is induced by both ALP-quark and ALP-gluon couplings. The pion and ALP interaction eigenstates π^0 , a are related to the mass eigenstates $\hat{\pi}^0$, \hat{a} via [28]⁵

$$\begin{aligned}\pi^0 &= \hat{\pi}^0 + \mathcal{O}\left(\frac{f_\pi^2}{f_a^2}\right) \\ a &= \hat{a} - \frac{1}{2\sqrt{2}} \frac{f_\pi}{f_a} \frac{m_\pi^2}{m_\pi^2 - m_a^2} \Delta c_{ud} \hat{\pi}^0 + \mathcal{O}\left(\frac{f_\pi^2}{f_a^2}\right),\end{aligned}\quad (3.9)$$

where $f_\pi \approx 130.5 \text{ MeV}$ is the pion decay constant and

$$\Delta c_{ud} = c_{uu}(\mu_{\text{chPT}}) - c_{dd}(\mu_{\text{chPT}}) + 2c_{GG} \frac{m_d - m_u}{m_d + m_u}. \quad (3.10)$$

The ALP-gluon coupling c_{GG} is scale-independent at least to two-loop order in the gauge couplings [28]. The ALP-quark couplings $c_{uu}(\mu_{\text{chPT}})$ and $c_{dd}(\mu_{\text{chPT}})$ are related to the couplings at the cutoff scale Λ of the ALP effective theory through the renormalization group. We apply the analytic evolution formulae from [28]. For $\Lambda = 4\pi \text{ TeV}$ and neglecting sub-leading contributions from electroweak ALP couplings, we obtain

$$\begin{aligned}c_{uu}(\mu_{\text{chPT}}) &\approx 0.98 c_{uu} - 0.12 c_{tt} - [3.6 c_{GG} + 1.2 c_{bb} + 1.8 (c_{dd} + c_{ss} + c_{cc})] \cdot 10^{-2}, \\ c_{dd}(\mu_{\text{chPT}}) &\approx 0.98 c_{dd} + 0.11 c_{tt} - [3.7 c_{GG} + 1.3 c_{bb} + 1.9 (c_{uu} + c_{ss} + c_{cc})] \cdot 10^{-2},\end{aligned}\quad (3.11)$$

where the couplings on the right-hand side are defined at the scale $\mu = \Lambda$.

The interactions of ALPs and pions with nucleons are described by the chiral Lagrangian [30, 50]

$$\mathcal{L}_{\text{chPT}} = \bar{\mathcal{N}} \left(i \not{D} - m_N \mathbf{1} + \frac{g_A}{2} \gamma^\mu \gamma_5 \mathbf{u}_\mu + \frac{g_0}{2} \gamma^\mu \gamma_5 \mathbf{u}_\mu^{(s)} \right) \mathcal{N}, \quad (3.12)$$

where $\mathcal{N} = (p, n)^T$ is the nucleon iso-doublet, $m_N = m_p \approx m_n$ is the nucleon mass, and $g_A \approx 1.25$ and $g_0 \approx 0.44$ are the external iso-vector and iso-scalar couplings [30, 51]. The various operators are defined by

$$\begin{aligned}i \mathbf{D}_\mu \mathcal{N} &= i(\partial_\mu + \mathbf{\Gamma}_\mu) \mathcal{N} \\ i \mathbf{\Gamma}_\mu &= \frac{1}{2} \left[\boldsymbol{\xi}(i\partial_\mu + \mathbf{r}_\mu) \boldsymbol{\xi}^\dagger + \boldsymbol{\xi}^\dagger (i\partial_\mu + \mathbf{l}_\mu) \boldsymbol{\xi} \right] + v_\mu^{(s)} \mathbf{1} \\ \mathbf{u}_\mu &= \boldsymbol{\xi}(i\partial_\mu + \mathbf{r}_\mu) \boldsymbol{\xi}^\dagger - \boldsymbol{\xi}^\dagger (i\partial_\mu + \mathbf{l}_\mu) \boldsymbol{\xi} \\ \mathbf{u}_\mu^{(s)} &= \frac{\partial_\mu a}{2f_a} (c_{uu} + c_{dd} + 2c_{GG}) \mathbf{1} \equiv 2a^{(s)} \frac{\partial_\mu a}{f_a} \mathbf{1}.\end{aligned}\quad (3.13)$$

The matrix $\boldsymbol{\xi}(x)$ is defined such that $\boldsymbol{\xi}^2(x) = \exp\left[\frac{i\sqrt{2}}{f_\pi} \boldsymbol{\sigma}^a \pi^a(x)\right]$, with pion fields π^a and Pauli matrices $\boldsymbol{\sigma}^a$. Here and in the remainder of this section, the ALP couplings c_{uu} and c_{dd} are evaluated at the scale μ_{chPT} , see (3.11).

⁵This relation holds for small mixing, $m_\pi^2/|m_\pi^2 - m_a^2| \lesssim f_a/f_\pi$. ALPs with masses close to the pion mass would induce large effects in well-tested pion interactions. Moreover, this relation is scheme-dependent; for details see Ref. [28].

The iso-vector chiral couplings of ALPs to nucleons are

$$\begin{aligned} \mathbf{r}_\mu &= \frac{\partial_\mu a}{f_a} \left[\frac{(\mathbf{c}_u - \mathbf{c}_d)_{11}}{2} + \frac{c_{GG}}{2} \frac{m_d - m_u}{m_d + m_u} + \frac{m_a^2}{m_\pi^2 - m_a^2} \frac{\Delta c_{ud}}{4} \right] \boldsymbol{\sigma}^3 \equiv \rho \frac{\partial_\mu a}{f_a} \boldsymbol{\sigma}^3 \\ \mathbf{l}_\mu &= \frac{\partial_\mu a}{f_a} \left[\frac{(\mathbf{c}_U - \mathbf{c}_D)_{11}}{2} - \frac{c_{GG}}{2} \frac{m_d - m_u}{m_d + m_u} - \frac{m_a^2}{m_\pi^2 - m_a^2} \frac{\Delta c_{ud}}{4} \right] \boldsymbol{\sigma}^3 \equiv \lambda \frac{\partial_\mu a}{f_a} \boldsymbol{\sigma}^3, \end{aligned} \quad (3.14)$$

and the iso-scalar vector coupling is

$$v_\mu^{(s)} = \frac{\partial_\mu a}{2f_a} \left[\frac{(\mathbf{c}_u + \mathbf{c}_d)_{11}}{2} + \frac{(\mathbf{c}_U + \mathbf{c}_D)_{11}}{2} \right] \equiv v^{(s)} \frac{\partial_\mu a}{2f_a}. \quad (3.15)$$

At leading order in $|\mathbf{q}|/f_a$ and $|\mathbf{q}|/f_\pi$, the chiral Lagrangian (3.12) includes interactions between neutral pions and nucleons

$$\mathcal{L}_{\text{chPT}} \supset \frac{g_A}{\sqrt{2}} \frac{\partial_\mu \pi^0}{f_\pi} (\bar{p} \gamma^\mu \gamma_5 p - \bar{n} \gamma^\mu \gamma_5 n), \quad (3.16)$$

as well as interactions between ALPs and nucleons

$$\begin{aligned} \mathcal{L}_{\text{chPT}} &\supset \frac{\partial_\mu a}{2f_a} \left(\bar{p} \gamma^\mu \left\{ v^{(s)} + (\rho + \lambda) + \left[g_A(\rho - \lambda) + 2g_0 a^{(s)} \right] \gamma_5 \right\} p \right. \\ &\quad \left. + \bar{n} \gamma^\mu \left\{ v^{(s)} - (\rho + \lambda) + \left[-g_A(\rho - \lambda) + 2g_0 a^{(s)} \right] \gamma_5 \right\} n \right) \\ &= \frac{\partial_\mu a}{2f_a} \left(\bar{p} \gamma^\mu \left\{ (\mathbf{c}_u + \mathbf{c}_U)_{11} + \frac{1}{2} g_{pa} \gamma_5 \right\} p + \bar{n} \gamma^\mu \left\{ (\mathbf{c}_d + \mathbf{c}_D)_{11} + \frac{1}{2} g_{na} \gamma_5 \right\} n \right), \end{aligned} \quad (3.17)$$

with the couplings

$$\begin{aligned} g_{pa} &= g_0(c_{uu} + c_{dd} + 2c_{GG}) + g_A \frac{m_\pi^2}{m_\pi^2 - m_a^2} \Delta c_{ud} \\ g_{na} &= g_0(c_{uu} + c_{dd} + 2c_{GG}) - g_A \frac{m_\pi^2}{m_\pi^2 - m_a^2} \Delta c_{ud}. \end{aligned} \quad (3.18)$$

Notice that (3.16) and (3.17) are given in terms of interaction states π^0, a . At leading order in f_π/f_a , the interactions with nucleons are identical to those of the mass states $\hat{\pi}^0, \hat{a}$.

Finally, the leading interactions of ALP and pion mass eigenstates with dark matter are described by

$$\mathcal{L}_{\text{chPT}-\chi} = \frac{c_\chi}{2f_a} \left(\partial^\mu \hat{a} - \frac{1}{2\sqrt{2}} \frac{f_\pi}{f_a} \frac{m_\pi^2}{m_\pi^2 - m_a^2} \Delta c_{ud} \partial^\mu \hat{\pi}^0 \right) \bar{\chi} \gamma_\mu \gamma_5 \chi. \quad (3.19)$$

The ALP-DM coupling c_χ is not renormalized, as long as dark-sector forces are weak.

In summary, ALP-pion mixing introduces interactions between pions and dark matter, see (3.19), as well as additional interactions between ALPs and nucleons, see (3.14), both proportional to Δc_{ud} . In section 4, we will use the interactions from (3.16) – (3.19) to calculate the amplitude for ALP-mediated dark matter-nucleon scattering at tree level.

3.3 Non-relativistic scattering

The non-relativistic (NR) limit of dark matter-nucleon scattering can be obtained by expanding the dark matter and nucleon currents in $|\mathbf{q}|/m$. For scalar and pseudo-scalar currents, this yields⁶

$$\begin{aligned}\bar{u}^{s'} u^s &\rightarrow \zeta^{s'\dagger} \zeta^s \\ \bar{u}^{s'}(p') i\gamma_5 u^s(p) &\rightarrow i(\mathbf{S})_{s's} \cdot \frac{\mathbf{p} - \mathbf{p}'}{m},\end{aligned}\tag{3.20}$$

with the spin matrix $(\mathbf{S})_{s's} = \zeta^{s'\dagger} \hat{\mathbf{S}} \zeta^s$, where the spin operator $\hat{\mathbf{S}} = \boldsymbol{\sigma}/2$ is directly proportional to the Pauli matrices $\boldsymbol{\sigma}$. The two-component spinors $\zeta^s, \zeta^{s'}$ fulfill the relation $\zeta^{s'\dagger} \zeta^s = \delta_{s's}$ with $s, s' = \{1, 2\}$. The Lagrangian for non-relativistic dark matter-nucleon scattering is then given by [47, 52]

$$\mathcal{L}_{\text{NR}} = \sum_{N=n,p} c_1^N \zeta_\chi^\dagger \zeta_N^\dagger \mathcal{O}_1^N \zeta_\chi \zeta_N + c_6^N \zeta_\chi^\dagger \zeta_N^\dagger \mathcal{O}_6^N \zeta_\chi \zeta_N + \dots,\tag{3.21}$$

with the relevant NR operators for elastic scattering

$$\begin{aligned}\mathcal{O}_1^N &= \mathbb{1}_\chi \mathbb{1}_N \\ \mathcal{O}_6^N &= \left[\hat{\mathbf{S}}_\chi \cdot \frac{\mathbf{q}}{m_N} \right] \left[\hat{\mathbf{S}}_N \cdot \frac{\mathbf{q}}{m_N} \right].\end{aligned}\tag{3.22}$$

For heavy ALPs, the coefficients in the NR Lagrangian (3.21) can be expressed in terms of the relativistic dark matter-nucleon interactions from (3.7),

$$\begin{aligned}c_1^N &= C_S^N \\ c_6^N &= \frac{m_N}{m_\chi} C_P^N.\end{aligned}\tag{3.23}$$

For light ALPs, the non-relativistic interactions must be calculated from the ALP-nucleon and ALP-dark matter interactions in (3.17) and (3.19). We will perform this calculation in section 4.

3.4 Dark matter-nucleus scattering

The differential cross section for dark matter-nucleus scattering can be expressed as [52]

$$\frac{d\sigma}{dE_R} = \frac{m_A}{2\pi v^2} \frac{4\pi}{2J_A + 1} \sum_{\tau, \tau'} \sum_O R_O^{\tau\tau'} W_O^{\tau\tau'}(|\mathbf{q}|),\tag{3.24}$$

where E_R , m_A , and J_A are the recoil energy, mass, and spin of the nucleus with mass number A , and v is the dark matter velocity in the Earth's rest frame. The nuclear response functions

$$W_O^{\tau\tau'}(|\mathbf{q}|) = \sum_J \langle J_A | O_{J,\tau} | J_A \rangle \langle J_A | O_{J,\tau'} | J_A \rangle, \quad \tau, \tau' = \{0, 1\},\tag{3.25}$$

⁶We use a non-relativistic normalization of currents; relativistic normalization would imply an extra factor $2m$.

are explicitly given in [52, 53]. Here the multipole operators $O = \{M, \Sigma', \Sigma'', \dots\}$ project onto the charge and the spin components of the nucleus. The indices $\tau, \tau' = \{0, 1\}$ denote the (strong) isospin components of the interaction, where 0 stands for isoscalar and 1 for isovector. In the isospin-conserving limit where dark matter interactions with protons and neutrons are identical, the spin-independent response functions of a nucleus with mass number A and atomic charge Z reduce to

$$\begin{aligned} W_M^{00} &= \kappa_A A^2 F^2(|\mathbf{q}|), & W_M^{11} &\rightarrow \kappa_A (A - 2Z)^2 F^2(|\mathbf{q}|) \\ W_M^{01} &= W_M^{10} = -\kappa_A A (A - 2Z) F^2(|\mathbf{q}|), \end{aligned} \quad (3.26)$$

with $\kappa_A = (2J_A + 1)/(4\pi)$ and $C(J_A) = \kappa_A (J_A + 1)/J_A$. The nuclear form factor $F(|\mathbf{q}|)$ parametrizes the decoherence in dark matter-nucleus scattering and is often approximated by the Helm form factor [54]. In the long-wavelength limit $|\mathbf{q}| \rightarrow 0$, coherent scattering off all nucleons occurs and $F(0) = 1$.

For a spin-dependent response, the response functions in the isospin and long-wavelength limit read

$$\begin{aligned} W_{\Sigma'}^{00} &= 4C(J_A)(S_p + S_n)^2, & W_{\Sigma'}^{11} &= 4C(J_A)(S_p - S_n)^2 \\ W_{\Sigma'}^{01} &= W_{\Sigma'}^{10} = 4C(J_A)(S_p^2 - S_n^2), \end{aligned} \quad (3.27)$$

where S_p and S_n are the spin averages of the protons and neutrons inside the nucleus. For ^{131}Xe , one has $S_p \approx -0.009$ and $S_n \approx -0.272$ [55]. In the long-wavelength limit, the spin-dependent response functions are related by $W_{\Sigma''}^{\tau\tau'} = W_{\Sigma'}^{\tau\tau'}/2$.

The nuclear response functions in (3.24) are weighted by the model-dependent factors $R_{\mathcal{O}}^{\tau\tau'}$, which encode the non-relativistic dark matter interaction with the nucleons. In particular, relativistic scalar and pseudo-scalar interactions induce spin-independent and spin-dependent non-relativistic scattering through [47, 52]

$$\begin{aligned} R_M^{\tau\tau'} &= c_1^\tau c_1^{\tau'} + \dots \\ R_{\Sigma''}^{\tau\tau'} &= \frac{1}{16} \frac{\mathbf{q}^4}{m_N^4} c_6^\tau c_6^{\tau'} + \dots, \end{aligned} \quad (3.28)$$

where the NR coefficients are expressed as linear combinations of c_i^p and c_i^n from eq. (3.21),

$$c_i^0 = \frac{1}{2}(c_i^p + c_i^n), \quad c_i^1 = \frac{1}{2}(c_i^p - c_i^n). \quad (3.29)$$

In the long-wavelength limit $1/|\mathbf{q}| \gg R_A$, where $R_A = 1.2A^{1/3}$ fm estimates the size of the nucleus, the differential cross section for specific scattering processes reduces to a compact analytical formula. For spin-independent interactions c_1^N , the differential dark matter-nucleus scattering cross section then reads

$$\frac{d\sigma_{\text{SI}}}{dE_R} \rightarrow \frac{m_A}{2\pi v^2} (Zc_1^p + (A - Z)c_1^n)^2. \quad (3.30)$$

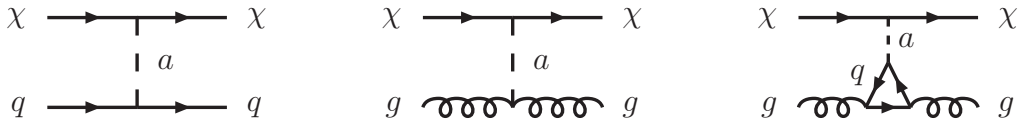


Figure 1: Feynman diagrams for ALP-mediated dark matter-quark scattering (left) and dark matter-gluon scattering (center and right) at $\mathcal{O}(c^2/f_a^2)$.

To compare with experimental results, we also define the average spin-independent scattering cross section per nucleon

$$\sigma_{\text{SI},N} = \frac{\mu_{\chi N}^2}{\pi} \left(\frac{Z}{A} c_1^p + \frac{A-Z}{A} c_1^n \right)^2, \quad (3.31)$$

with the dark matter-nucleon reduced mass $\mu_{\chi N} = m_N m_\chi / (m_N + m_\chi)$.

For spin-dependent interactions c_6^N , the differential dark matter-nucleus scattering cross section in the long-wavelength limit is

$$\frac{d\sigma_{\text{SD}}}{dE_R} \rightarrow \frac{m_A}{4\pi v^2} \frac{J_A + 1}{J_A} \left(\frac{m_A E_R}{m_N^2} \right)^2 (c_6^p S_p + c_6^n S_n)^2. \quad (3.32)$$

Notice that spin-dependent scattering is suppressed at small recoil energy, $E_R \rightarrow 0$.

The expected scattering event rate per unit detector mass can finally be computed using the differential cross section via

$$\frac{dR}{dE_R} = \frac{\rho_\chi}{m_A m_\chi} \int_{v_{\text{min}}} \frac{d\sigma}{dE_R} v f_\oplus(\mathbf{v}) d^3\mathbf{v}, \quad (3.33)$$

where ρ_χ is the local dark matter density, $f_\oplus(\mathbf{v})$ is the dark matter velocity distribution in the Earth's rest frame [56], and $v_{\text{min}} = \sqrt{m_A E_R / 2} / \mu_{\chi A}$ with the reduced mass $\mu_{\chi A} = m_A m_\chi / (m_A + m_\chi)$.

4 Tree level: spin-dependent scattering

Based on the formalism from section 3, we calculate the dominant contributions to non-relativistic dark matter-nucleus scattering through the exchange of heavy and light ALPs. As anticipated, ALP exchange at tree level induces purely spin-dependent scattering. In section 5, we will analyze spin-independent, loop-induced scattering.

4.1 Heavy ALP mediator

At tree level, ALP exchange between the dark matter particles and the nucleon constituents, shown in fig. 1, generates pseudo-scalar interactions with quarks and interactions with the gluon configuration $G\tilde{G}$. We integrate out the ALP at the scale $\mu = m_a$. In terms of the

effective ALP couplings from (2.1), the Wilson coefficients from (3.1) read

$$\begin{aligned} C_P^q(m_a) &= \frac{m_\chi c_\chi c_{qq}(m_a)}{m_a^2 f_a^2}, \\ C_{\tilde{G}}(m_a) &= -2 \frac{m_\chi c_\chi}{m_a^2 f_a^2} \left[c_{GG} + \frac{1}{2} \sum_Q c_{QQ}(m_a) \Theta(m_a - m_Q) \right]. \end{aligned} \quad (4.1)$$

Here we have included the one-loop quark contribution to $C_{\tilde{G}}$ (fig. 1, right), where the sum runs over all quarks Q which are lighter than the ALP.

As mentioned in Sec. 3.1, the coefficients C_P^q and $C_{\tilde{G}}$ are not renormalized when evolved to lower scales [49]. The only effects are threshold corrections as the energy scale crosses the mass threshold of the various quarks, see (3.4). These threshold corrections remove the c_{QQ} contribution of the respective quark from $C_{\tilde{G}}$ in (4.1). Integrating out the charm quark at $\mu = \mu_{\text{chPT}}$, the low-scale Wilson coefficients for dark matter interactions due to heavy-ALP exchange are given by

$$\begin{aligned} C_P^q(\mu_{\text{chPT}}) &= \frac{m_\chi c_\chi c_{qq}(m_a)}{m_a^2 f_a^2}, \\ C_{\tilde{G}}(\mu_{\text{chPT}}) &= -2 \frac{m_\chi c_\chi}{m_a^2 f_a^2} \left[c_{GG} + \frac{1}{2} \sum_{q=u,d,s} c_{qq}(m_a) \right]. \end{aligned} \quad (4.2)$$

The scalar interaction C_S^q is only generated at loop level, see section 5. Using the chiral matching conditions from (3.7) and the relations from (3.23), we match the effective couplings in (4.2) to the non-relativistic dark matter-nucleon interactions. The result is a spin-dependent NR interaction

$$c_6^N(q^2) = \frac{m_N c_\chi}{m_a^2 f_a^2} \left[\sum_{q=u,d,s} c_{qq}(m_a) F_P^{q/N}(q^2) - \left(2c_{GG} + \sum_{q=u,d,s} c_{qq}(m_a) \right) F_{\tilde{G}}^N(q^2) \right]. \quad (4.3)$$

As the form factors $F_P^{q/N}(q^2)$ and $F_{\tilde{G}}^N(q^2)$ are numerically of the same order, the dark matter-gluon interaction via a quark loop is of similar strength as the tree-level dark matter-quark interaction.

The cross section for ALP-mediated dark matter-nucleus scattering at tree level can finally be obtained by inserting c_6^N from (4.3) into (3.32).

4.2 Light ALP mediator

For ALPs with masses $m_a < \mu_{\text{chPT}}$, dark matter can scatter with nucleons via the tree-level diagrams shown in fig. 2. The matrix element for relativistic dark matter scattering off protons via $\chi p \rightarrow \chi p$ is

$$\begin{aligned} \mathcal{M}_{\text{tree}} &= -\frac{g_{pa} m_N m_\chi c_\chi}{2 f_a^2} \frac{1}{q^2 - m_a^2} (\bar{u}_\chi i \gamma_5 u_\chi) (\bar{u}_p i \gamma_5 u_p) \\ &+ \frac{g_A m_N m_\chi c_\chi}{2 f_a^2} \frac{1}{q^2 - m_\pi^2} \frac{m_\pi^2}{m_\pi^2 - m_a^2} \Delta c_{ud} (\bar{u}_\chi i \gamma_5 u_\chi) (\bar{u}_p i \gamma_5 u_p). \end{aligned} \quad (4.4)$$

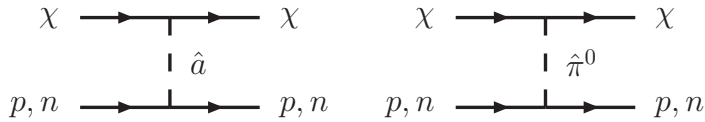


Figure 2: Feynman diagrams for tree-level ALP-mediated and pion-mediated dark matter-nucleon scattering at $\mathcal{O}(c^2/f_a^2)$.

The amplitude for scattering off neutrons, $\chi n \rightarrow \chi n$, is obtained by replacing $p \rightarrow n$ and $\Delta c_{ud} \rightarrow -\Delta c_{ud}$ in (4.4). This result is different from that of Ref. [57], where ALP-pion mixing was not considered. Matching (4.4) onto the non-relativistic amplitude, we determine the spin-dependent dark matter-nucleon interaction in (3.21) for protons and neutrons to be

$$\begin{aligned}
 c_6^p(\mathbf{q}^2) &= \frac{c_\chi}{2f_a^2} m_N^2 \left[\frac{g_{pa}}{\mathbf{q}^2 + m_a^2} - \frac{g_A}{\mathbf{q}^2 + m_\pi^2} \frac{m_\pi^2}{m_\pi^2 - m_a^2} \Delta c_{ud} \right] \\
 c_6^n(\mathbf{q}^2) &= \frac{c_\chi}{2f_a^2} m_N^2 \left[\frac{g_{na}}{\mathbf{q}^2 + m_a^2} + \frac{g_A}{\mathbf{q}^2 + m_\pi^2} \frac{m_\pi^2}{m_\pi^2 - m_a^2} \Delta c_{ud} \right].
 \end{aligned} \tag{4.5}$$

In the limit $m_a \rightarrow 0$, the interactions feature the typical $1/\mathbf{q}^2$ behavior of a massless mediator.

5 Loop level: spin-independent scattering

Owing to the pseudo-scalar nature of the ALP, tree-level scattering is subject to both spin and momentum suppression. At the one-loop level, both types of suppression can be lifted through diagrams involving two ALP insertions. Such loop-induced processes generate *scalar* dark matter-nucleon interactions, which are finite at small momentum exchange and induce coherent spin-independent scattering, but come at the price of a loop suppression. For heavy nuclei, coherent scalar interactions are enhanced by a factor of $A^2(m_N/|\mathbf{q}|)^4$, see (3.28) and (3.30), compared to spin-dependent pseudo-scalar interactions. A priori, it seems plausible that loop-induced scattering could dominate over ALP-mediated tree-level scattering.

In this section, we will analyze three different classes of loop contributions that generate scalar dark matter-nucleon interactions. The first class, discussed in section 5.1, involves flavor-diagonal ALP couplings to quarks. The corresponding loop diagram shown in fig. 3, left, induces scalar interactions of dark matter with valence quarks and with the gluon condensate inside the nucleon.

The second class, discussed in section 5.2, involves loops with flavor-changing neutral currents of ALPs coupling to virtual top quarks and valence up quarks, see fig. 3, right. The large top mass leads to strongly enhanced scalar dark matter-nucleon interactions compared to flavor-diagonal contributions. For ALP masses $m_a > \mu_{\text{chPT}}$, both classes of one-loop amplitudes can be matched onto the effective Lagrangian (3.5) that describes dark matter-nucleon interactions at leading order in chiral perturbation theory.

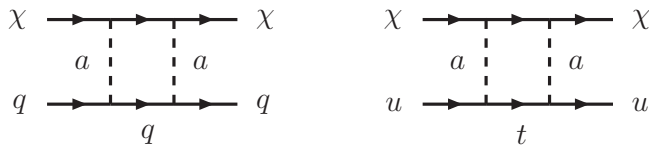


Figure 3: Feynman diagrams for loop-induced dark matter-quark scattering via flavor-diagonal (left) and flavor-changing (right) ALP couplings at $\mathcal{O}(c^4/f_a^4)$. Crossed diagrams also contribute to the scattering amplitude.

In a third class of contributions, discussed in section 5.3, the spin suppression of tree-level scattering is lifted at loop level in chiral perturbation theory. Unlike in the previous cases, for ALP masses $m_a > \mu_{\text{chPT}}$ the *tree-level* scattering amplitude is matched onto the effective Lagrangian (3.5). The scalar dark matter-nucleon interaction is then generated by loop diagrams with virtual pion exchange, see fig. 4.

As we will see, loop-induced dark matter-nucleon scattering through ALPs results in scattering rates that can be probed by current and upcoming direct detection experiments. Notice that scalar dark matter-nucleon scattering can also be generated by heavy mediators with masses above the cutoff scale of the ALP effective theory, see e.g. [19]. Such contributions are model-dependent, but could compete with the generic contributions discussed in this work. We will not include them in what follows.

Throughout this section, we will assume that $m_a > \mu_{\text{chPT}}$, such that the ALP can be integrated out before matching onto the chiral Lagrangian. For $m_a < \mu_{\text{chPT}}$, the loop calculations would need to be carried out in the chiral effective theory of ALP-nucleon interactions described in section 3.2. Phenomenologically, the case of light ALPs is less relevant, since strong experimental constraints on sub-GeV ALPs suppress dark matter-nucleon scattering way beyond observation at current and upcoming direct detection experiments.

5.1 Flavor-diagonal ALP couplings

For ALPs with flavor-diagonal couplings to quarks, we calculate the loop-induced amplitude for $\chi q \rightarrow \chi q$ scattering from the left diagram in fig. 3, plus the corresponding diagram with crossed ALP couplings to the quark line. Only the axial-vector couplings of the ALP to up and down quarks, $c_{uu} = (\mathbf{c}_u - \mathbf{c}_U)_{11}$ and $c_{dd} = (\mathbf{c}_d - \mathbf{c}_D)_{11}$, contribute, see (2.2). The vector part $(\mathbf{c}_q + \mathbf{c}_Q)_{ii}$ does not contribute, because the remaining couplings involved in the amplitude conserve the flavor-diagonal vector current $\bar{q}\gamma_\mu q$. Our result for the relativistic one-loop scattering amplitude can be found in (A.1) of section A.

For general external momenta, the amplitude contains only scalar and vector dark matter-quark interactions. Indeed, the two γ_5 insertions from the ALP-quark couplings prevent pseudo-scalar or axial-vector structures. The scalar contribution arises from the quark mass insertion m_q on the propagator of the virtual quark in the loop, plus momentum contributions of external on-shell quarks, which reduce to m_q when applying the Dirac equation. The same holds for the dark matter current. The vector contribution is generated

only from momentum contributions that cannot be reduced by applying the Dirac equation on external states.

In the limit where the mass and momentum of the external quarks can be neglected with respect to the ALP mass, that is $m_q, |\mathbf{k}|, |\mathbf{k}'| \ll m_a$, we obtain the scattering amplitude in D dimensions as

$$\mathcal{M}_{\text{loop}}^{\text{FD}}(\mu) = \frac{m_q m_\chi c_\chi^2 c_{qq}^2(\mu)}{32\pi^2 f_a^4} (\bar{u}_\chi u_\chi)(\bar{u}_q u_q) \left[\Delta - \ln\left(\frac{m_a^2}{\mu^2}\right) + L_{\text{FD}}(m_a, m_\chi) \right], \quad (5.1)$$

with $q = \{u, d\}$ and the loop function

$$L_{\text{FD}}(m_a, m_\chi) = 2 + \frac{(m_\chi^2 - m_a^2) \ln(m_a^2/m_\chi^2)}{m_\chi^2} - \frac{2m_a(3m_\chi^2 - m_a^2) \ln\left(\frac{m_a + \sqrt{m_a^2 - 4m_\chi^2}}{2m_\chi}\right)}{m_\chi^2 \sqrt{m_a^2 - 4m_\chi^2}}. \quad (5.2)$$

The result is UV-divergent in 4 dimensions, as is apparent from $\Delta = 2/(4-D) - \gamma_E + \log(4\pi)$ and the remnant dependence on the renormalization scale μ . We renormalize the amplitude in the $\overline{\text{MS}}$ scheme at the scale $\mu = m_a$ by absorbing the divergence Δ into a $\bar{\chi}\chi\bar{q}q$ counterterm generated by the UV completion of the ALP effective theory (2.1). We neglect potential model-dependent contributions that could be induced by heavy particles above the cutoff scale of the ALP effective theory.

For $m_a \gg m_q$, the loop-induced dark matter-quark scattering can be considered as a contact interaction and the formalism from section 3.1 applies. Matching the renormalized amplitude (5.1) onto the effective Lagrangian (3.1) at $\mu = m_a$ and evolving the Wilson coefficients down to the scale of chiral symmetry breaking using (3.4), we obtain

$$\begin{aligned} C_S^q(\mu_{\text{chPT}}) &= \frac{m_\chi c_\chi^2 c_{qq}^2(m_a)}{32\pi^2 f_a^4} L_{\text{FD}}(m_a, m_\chi) \quad \text{for } q = \{u, d, s\}, \\ C_G(\mu_{\text{chPT}}) &= -\frac{m_\chi c_\chi^2}{32\pi^2 f_a^4} L_{\text{FD}}(m_a, m_\chi) \sum_Q c_{QQ}^2(m_a). \end{aligned} \quad (5.3)$$

The sum is over all quarks Q with $\mu_{\text{chPT}} < m_Q < m_a$. Notice that C_G is purely induced by quark threshold corrections, see (3.3). We match these coefficients onto chiral perturbation theory using (3.7) and obtain

$$C_S^N(q^2 < \mu_{\text{chPT}}^2) = \left(\sum_{q=u,d,s} c_{qq}^2(m_a) F_S^{q/N}(q^2) - \sum_Q c_{QQ}^2(m_a) F_G^N(q^2) \right) \frac{m_\chi c_\chi^2}{32\pi^2 f_a^4} L_{\text{FD}}(m_a, m_\chi), \quad (5.4)$$

where again $\mu_{\text{chPT}} < m_Q < m_a$. In the non-relativistic limit $|\mathbf{q}|/m_{\chi,N} \ll 1$, the Wilson coefficient can be readily identified with the coefficient for spin-independent scattering, $c_1^N = C_S^N$, see (3.23).

In the limit of zero momentum transfer, $q^2 = 0$, the nucleon form factors are approximated by [47]

$$F_S^{q/N}(0) \approx (0.02 - 0.04) m_N, \quad F_G^N(0) \approx -0.06 m_N, \quad (5.5)$$

where the quark form factor varies between 0.02 and 0.04, depending on the type of valence quark and nucleon. For similar ALP couplings $c_{qq} \approx c_{QQ}$, contributions from light and heavy quarks to the spin-independent scattering coefficient c_1^N are numerically of the same order. Notice that both contributions add up constructively; cancellations between dark matter interactions with valence quarks and gluons do not occur.

In the limit $m_a \gg m_q, m_\chi$, loop-induced scalar interactions from FD ALP-quark couplings scale as $m_\chi m_N (m_\chi^2/m_a^2)/(32\pi^2 f_a^4)$. The decoupling for $m_\chi/m_a \rightarrow 0$ and the strong suppression by the cutoff scale of the ALP effective theory indicate a small contribution to the scattering rate.

Besides the dark matter-quark loop contributions from fig. 3, effective ALP couplings to gluons can generate similar box diagrams to fig. 3, left, where the quarks are replaced by gluons. In many models, effective ALP-gluon couplings are generated at the loop level, as suggested by the coupling definition in (2.1). The resulting loop-induced dark matter-gluon interactions are therefore suppressed compared to the DM-quark interactions. We do not discuss loop-induced dark matter-gluon interactions in this work.

5.2 Flavor-changing ALP couplings

Compared to the case of flavor-diagonal couplings from section 5.1, loop-induced dark matter-nucleon scattering with flavor-changing ALP couplings is strongly enhanced if the virtual quark in the loop is much heavier than the valence quarks inside the nucleon. In particular, for ALPs with flavor-changing couplings to up quarks and top quarks, the $\chi u \rightarrow \chi u$ scattering amplitude receives contributions with a virtual top quark from the right diagram in fig. 3, plus the corresponding crossed diagram. Both the vector coupling c_{ut}^V and the axial-vector coupling c_{ut}^A of the ALP, defined in (2.5), contribute. The large top mass induces a quark chirality flip, which generates a scalar current scaling as $(m_t/f_a) \bar{u}u$. The amplitude for spin-independent dark matter-nucleon scattering through FC couplings is therefore enhanced by a factor m_t/m_u compared to the FD case. This top-mass enhancement partially lifts the suppression by f_a . A similar mechanism has been observed for ALP-induced electromagnetic dipole moments with FC couplings to top quarks [58].

For general external momenta, the dark matter-quark scattering amplitude includes all four types of Lorentz structures: scalar, pseudo-scalar, vector and axial-vector. However, only scalar and vector structures induce spin-independent coherent dark matter-nucleus scattering. We therefore neglect the pseudo-scalar and axial-vector interactions in this discussion. Our result for the full relativistic one-loop scattering amplitude can be found in (A.3) of section A.

For external momenta much smaller than the top-quark mass as well as the ALP mass, $|\mathbf{k}|, |\mathbf{k}'| \ll m_t, m_a$, and neglecting contributions of $\mathcal{O}(m_u/m_t)$, the amplitude for $\chi u \rightarrow \chi u$

scattering through FC ALP couplings simplifies to

$$\mathcal{M}_{\text{loop}}^{\text{FC}}(\mu) = \frac{m_\chi m_t}{64\pi^2 f_a^4} c_\chi^2 \left[|c_{ut}^V|^2(\mu) - |c_{ut}^A|^2(\mu) \right] (\bar{u}_\chi u_\chi)(\bar{u}_u u_u) \quad (5.6)$$

$$\cdot \left[-\Delta + \ln\left(\frac{m_t^2}{\mu^2}\right) + L_{\text{FC}}(m_\chi, m_a, m_t) \right],$$

where

$$L_{\text{FC}}(m_\chi, m_a, m_t) = \frac{1}{(m_t^2 - m_a^2)^2} \left[m_a^2 (2m_t^2 - m_a^2) b_0(m_a, m_\chi) - m_t^4 b_0(m_t, m_\chi) \right. \\ \left. + m_a^4 (m_t^2 - m_a^2) \frac{d}{dm_a^2} b_0(m_a, m_\chi) \right] + \ln\left(\frac{m_\chi^2}{m_t^2}\right),$$

$$b_0(m_i, m_\chi) = 2 - \frac{m_i^2}{2m_\chi^2} \ln\left(\frac{m_i^2}{m_\chi^2}\right) + \frac{m_i \sqrt{m_i^2 - 4m_\chi^2}}{m_\chi^2} \ln\left(\frac{m_i + \sqrt{m_i^2 - 4m_\chi^2}}{2m_\chi}\right), \quad (5.7)$$

with $i = \{t, a\}$. Notice that the amplitude in (5.6) is proportional to the combination of couplings $|c_{ut}^V|^2 - |c_{ut}^A|^2$. In the case of purely chiral ALP-quark couplings, where either $(\mathbf{c}_U)_{13} \rightarrow 0$ or $(\mathbf{c}_u)_{13} \rightarrow 0$, the momentum-independent amplitude from (5.6) vanishes. In that case, the scattering amplitude is lead by terms suppressed as $|\mathbf{k}|/m_t$, $|\mathbf{k}'|/m_t$ or m_u/m_t compared to (5.6), see section A. We expect these contributions to be of similar order as the FD amplitude from (5.1).

As in the flavor-diagonal case, the FC amplitude from (5.6) is UV-divergent. Also here, we renormalize the amplitude in the MS-bar scheme using a $\bar{\chi}\chi\bar{u}u$ counterterm. For ALP masses $m_a < m_t$, we choose $\mu = m_a$ as renormalization scale, as this is the scale where the $\bar{\chi}\chi\bar{u}u$ contact interaction is generated upon integrating out the virtual particles. For $m_a > m_t$, we choose $\mu = m_t$.

Let us focus here on the case $m_a > m_t$. Evolving the flavor-changing ALP couplings from the cutoff scale $\Lambda = 4\pi \text{ TeV}$ down to the matching scale $\mu = m_t$ [28], we find

$$c_{ut}^V(m_t) \approx 0.984 c_{ut}^V(\Lambda) - 0.005 c_{ut}^A(\Lambda),$$

$$c_{ut}^A(m_t) \approx -0.005 c_{ut}^V(\Lambda) + 0.984 c_{ut}^A(\Lambda). \quad (5.8)$$

At the scale $\mu = m_t$, we match the renormalized FC amplitude onto the effective Lagrangian for DM-quark interactions from eq. (3.1).⁷ Following the procedure described in section 3.1, we calculate the Wilson coefficient for scalar dark matter-nucleon interactions by matching the effective DM-quark interaction onto the dark matter-nucleon effective theory at $\mu = \mu_{\text{chPT}}$ using eq. (3.7). We find

$$C_S^N(q^2 < \mu_{\text{chPT}}^2) = F_S^{u/N}(q^2) \frac{m_t}{m_u} \frac{m_\chi}{64\pi^2 f_a^4} c_\chi^2 \left[|c_{ut}^V|^2(m_t) - |c_{ut}^A|^2(m_t) \right] L_{\text{FC}}(m_\chi, m_a, m_t). \quad (5.9)$$

⁷To be precise, one would first integrate out the ALP and subsequently the top quark. We neglect this extra step and integrate out both particles at $\mu = m_t$, since the scale separation between $\mu = m_a < 4\pi f_a$ and $\mu = m_t$ is moderate. This allows us to express the ALP-quark couplings $c_{ut}^V(m_t)$ and $c_{ut}^A(m_t)$ in terms of ALP couplings at the cutoff scale Λ .

As anticipated, the scalar interaction from FC ALP couplings is enhanced by m_t/m_u compared to the FD case (5.4). The coefficient for non-relativistic spin-independent scattering can be easily obtained by identifying $c_1^N = C_S^N$, see (3.23).

In the limit $m_\chi \gg m_a, m_t$, the effective scalar coupling C_S^N scales as $m_\chi \ln(m_\chi^2/m_t^2)$. Dark matter scattering through FC ALP couplings is therefore significantly enhanced at large dark matter masses. On the other hand, in the limit $m_a \gg m_\chi, m_t$ the scalar coupling scales as $\ln(m_a^2/m_t^2)$, yielding a mild logarithmic dependence on the ALP mass.

5.3 Pion loops in chiral perturbation theory

In the previous two sections, scalar dark matter-nucleon interactions were generated by matching the ALP effective theory onto chiral perturbation theory at the one-loop level. But a scalar contact interaction can also be generated from loop diagrams *within* chiral perturbation theory. While the tree-level matching of an ALP-quark interaction onto the chiral Lagrangian generates a pseudo-scalar dark matter-nucleon interaction, at loop level one can construct a scalar interaction via the exchange of a neutral pion or eta meson. However, the price to pay for turning a pseudo-scalar interaction into a scalar interaction is a chiral loop suppression. As we will show in this section, this suppression renders loop contributions in chiral perturbation theory subdominant compared to the contributions discussed in the previous sections.

In fig. 4, we show Feynman diagrams in chiral perturbation theory that result in a scalar $\bar{\chi}\chi\bar{N}N$ interaction. The ALP is considered heavy compared to the scale of chiral symmetry breaking, $m_a > \mu_{\text{chPT}}$, leading to effective dark matter-hadron interactions and nucleon-meson interactions. To generate a scalar dark matter-nucleon interaction, the pion or eta meson must be emitted from the nucleon and connected to the dark matter line, in a way to ensure an even number of γ_5 insertions on the nucleon lines. In this section, we discuss only pion-mediated processes for simplicity. Diagrams involving the eta meson are enhanced by the large meson mass, but not enough to change the conclusions.

Since the energy scale of dark matter-nucleon scattering is much smaller than both the dark matter mass and the nucleon mass, one can work with an effective theory of heavy dark matter and heavy baryon interactions, formulated as the Heavy Dark Matter Effective Theory (HDMEFT) [59–61] and the Heavy Baryon Chiral Perturbation Theory (HBChPT) [62–65], respectively. The main approach to HDMEFT or HBChPT is the same. The Dirac field ψ of the heavy particle with mass m and momentum $p = mv + \tilde{p}$, where v^μ is the four-velocity of the heavy particle and $\tilde{p} \ll mv$, is decomposed into particle and antiparticle components h and H , so that

$$\psi(x) = e^{-imvx}[h(x) + H(x)], \quad (5.10)$$

where

$$h(x) = e^{imvx} \frac{1 + \not{v}}{2} \psi(x), \quad H(x) = e^{imvx} \frac{1 - \not{v}}{2} \psi(x). \quad (5.11)$$

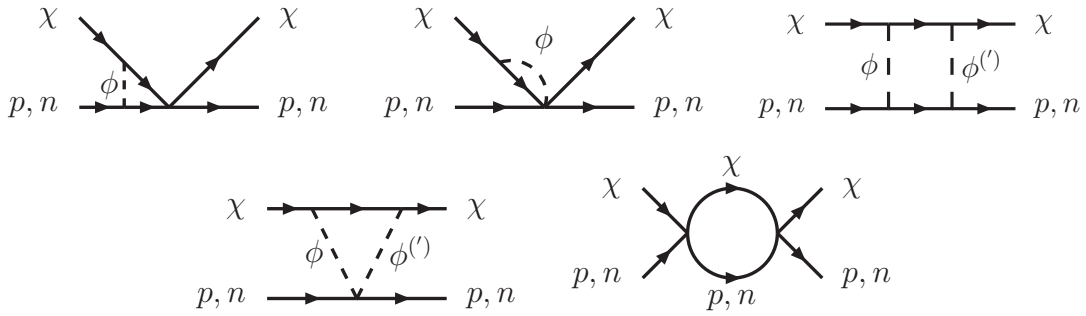


Figure 4: Feynman diagrams for loop-induced ALP-mediated dark matter-nucleon scattering with neutral meson exchange at $\mathcal{O}(c^4/f_a^4)$, where $\phi, \phi' = \pi^0, \eta$. Scalar $\chi\chi NN$ interactions are generated through various ALP-induced effective couplings in chiral perturbation theory: a $\chi\chi NN$ contact interaction (top left, bottom right), a $\chi\chi NN\phi$ contact interaction (top middle), two-meson exchange (top right), and a $NN\phi\phi^{(\prime)}$ contact interaction (bottom left).

At energies below the particle-antiparticle production threshold, one can integrate out the antiparticle component $H(x)$ to obtain an effective Lagrangian with the kinetic terms [63, 66]

$$\begin{aligned}\mathcal{L}_{\text{eff}} &= \bar{h} i v \cdot \partial h + \bar{h} i \not{\partial}_{\perp} (i v \cdot \partial + 2m - i\epsilon)^{-1} i \not{\partial}_{\perp} h \\ &= \bar{h} i v \cdot \partial h + \mathcal{O}(\tilde{p}/m),\end{aligned}\tag{5.12}$$

where $\gamma_{\perp}^{\mu} = \gamma^{\mu} - v^{\mu} \not{v}$. Consequently, the propagator of the heavy Dirac field $h(x)$ is $i/v \cdot \tilde{p}$. Without loss of generality, we choose the four-velocity of the heavy particle to be $v^{\mu} = (1, \mathbf{0})$ [63]. We do this for both the dark matter particle and the nucleon, which is justified since the momentum exchange between them is of $\mathcal{O}(\tilde{p}/m)$. If the heavy particle is on-shell, its propagator is inversely proportional to its kinetic energy.

Integrating out the antiparticle modes H in the interaction terms of the chiral Lagrangian, we have [40]⁸

$$\begin{aligned}\mathcal{L} \supset & \frac{C_{p\pi}}{f_{\pi}} (\bar{p} i q \cdot S_p p) \pi^0 - \frac{C_{p\pi\pi}}{2f_{\pi}} (\bar{p} p) (\pi^0)^2 + \left(\frac{m_{\pi}^3}{m_{\chi}} C_{\chi\pi,0} - \frac{m_{\pi}}{m_{\chi}} q^2 C_{\chi\pi,1} \right) (\bar{\chi} i q \cdot S_{\chi} \chi) \pi^0 \\ & + \frac{C_{\chi p}}{m_{\chi}} (\bar{\chi} i q \cdot S_{\chi} \chi) (\bar{p} i q \cdot S_p p) - \frac{C_{\chi p\pi}}{m_{\chi}} (\bar{\chi} i q \cdot S_{\chi} \chi) (\bar{p} p) \pi^0 + (p \rightarrow n, u \leftrightarrow d).\end{aligned}\tag{5.13}$$

⁸Compared to [40], we have added the interaction term $NN\pi\pi$ that can be derived from, for example, [67]. Our convention for the transformation properties of the meson field matrix Σ , see eq. (2.26), follows that of [28], which differs from [40] by hermitian conjugation. This results in a minus sign for the meson fields in the Lagrangian relative to [40].

Here, we have defined $S^\mu = \gamma_\perp^\mu \gamma_5 / 2$. The coefficients are given by

$$\begin{aligned}
C_{p\pi} &= (-1)^{Q_p} \sqrt{2} (D + F), \\
C_{p\pi\pi} &= \frac{4}{f_\pi} [b_0 m_d + (b_0 + b_D + b_F) m_u], \\
C_{\chi\pi,0} &= \frac{B_0 f_\pi}{m_\pi^3 \sqrt{2}} (m_u C_P^u - m_d C_P^d), \\
C_{\chi\pi,1} &= \frac{\tilde{m}}{2\sqrt{2}} \left(\frac{1}{m_u} - \frac{1}{m_d} \right) \frac{f_\pi}{m_\pi} C_{\tilde{G}}, \\
C_{\chi p} &= \left[D \left(\frac{\tilde{m}}{m_u} + \frac{\tilde{m}}{m_s} \right) + F \left(\frac{\tilde{m}}{m_u} - \frac{\tilde{m}}{m_s} \right) + G \right] C_{\tilde{G}}, \\
C_{\chi p\pi} &= (-1)^{Q_p} \frac{2\sqrt{2}}{f_\pi} \left[(b_0 + b_D + b_F) m_u C_P^u - b_0 m_d C_P^d \right], \tag{5.14}
\end{aligned}$$

with $\tilde{m} = (1/m_u + 1/m_d + 1/m_s)^{-1}$ and the low-energy constants $D = 0.812(30)$, $F = 0.462(14)$, $G = -0.376(28)$, $B_0 m_u = (6.2 \pm 0.4) \cdot 10^{-3} \text{ GeV}^2$, $B_0 m_d \approx (13.3 \pm 0.4) \cdot 10^{-3} \text{ GeV}^2$, $b_0 = -3.7 \pm 1.4$, $b_D = 1.4 \pm 0.8$, $b_F = -1.8 \pm 0.8$ [40, 68, 69]. The Wilson coefficients of the effective dark matter-gluon and dark matter-quark interactions, $C_{\tilde{G}}$, C_P^u and C_P^d , were defined in eq. (4.2). Using the central values for the low-energy constants, we have

$$\begin{aligned}
C_{p\pi} &\approx -1.80, \\
C_{p\pi\pi} &\approx -0.81, \\
C_{\chi\pi,0} &\approx 0.23 C_P^u(\mu_{\text{chPT}}) - 0.50 C_P^d(\mu_{\text{chPT}}), \\
C_{\chi\pi,1} &\approx 0.12 C_{\tilde{G}}(\mu_{\text{chPT}}), \\
C_{\chi p} &\approx 0.48 C_{\tilde{G}}(\mu_{\text{chPT}}), \\
C_{\chi p\pi} &\approx 0.20 C_P^u(\mu_{\text{chPT}}) - 0.38 C_P^d(\mu_{\text{chPT}}). \tag{5.15}
\end{aligned}$$

In this normalization convention, the Wilson coefficients of the chiral effective theory are either dimensionless constants of order one, or products of a dimensionless order-one constant and a Wilson coefficient of dark matter scattering with quarks and gluons. This choice allows us to separate the suppression of $1/(m_a^2 f_a^2)$ captured in the high-energy coefficients C_P^q and $C_{\tilde{G}}$ from the momentum and pion-mass suppression in chiral perturbation theory.

All diagrams shown in fig. 4 are of order $\mathcal{O}(c^4/f_a^4)$, just as the perturbative one-loop contributions from section 5.1 and section 5.2. However, the chPT contributions are further suppressed by powers of $q/m_{\chi,N}$ and $m_\pi/m_{\chi,N}$. To estimate this suppression, we introduce a power counting scheme that takes account of the fact that all chPT coefficients in eq. (5.14) are of similar magnitude. In the effective Lagrangian eq. (5.13), we treat the coefficients $C_{p\pi}, C_{p\pi\pi}$ as $\mathcal{O}(1)$ and $C_{\chi\pi,0}, C_{\chi\pi,1}, C_{\chi p}, C_{\chi p\pi}$ as $\mathcal{O}(c^2/f_a^2)$, and count additional pre-factors as $m_\pi \sim f_\pi \sim q$. In this scheme, the coupling strength of the vertex $NN\pi$ is of order $\mathcal{O}(1)$, $NN\pi\pi$ is of order $\mathcal{O}(1/q)$, $\chi\chi\pi$ is of order $\mathcal{O}(q^4/m_\chi \times c^2/f_a^2)$, $\chi\chi NN$ is of order $\mathcal{O}(q^2/m_\chi \times c^2/f_a^2)$, and $\chi\chi NN\pi$ is of order $\mathcal{O}(q/m_\chi \times c^2/f_a^2)$. This order-of-magnitude estimate differs from the formal power counting often used in chiral perturbation theory,

for instance in [40].⁹ Nevertheless, both power counting schemes give the same qualitative conclusion.

In two-particle-irreducible diagrams, such as the second and fourth diagram in fig. 4, each loop integration yields a factor of $\mathcal{O}(q^4/(16\pi^2))$, while each fermion or meson propagator contributes as $\mathcal{O}(1/q)$ or $\mathcal{O}(1/q^2)$, respectively. In two-particle-reducible diagrams such as the first, third and last diagram in fig. 4, the internal heavy fermion lines can be put on-shell, with a kinetic energy of order $\mathcal{O}(q^2/m_{\chi,N})$. In that case, the power counting needs to be modified as suggested in [70–72]: each nucleon or dark matter propagator that can be on-shell contributes as $\mathcal{O}(m_{\chi,N}/q^2)$, each loop integral contributes $\mathcal{O}(q^5/(16\pi^2 m_N))$. With these two kinds of counting, we determine the leading contribution of each diagram type in fig. 4 as

$$\begin{aligned} \text{Type 1 : } & \frac{c^4}{f_a^4} \frac{q^5}{16\pi^2 m_\chi}, & \text{Type 2 : } & \frac{c^4}{f_a^4} \frac{q^6}{16\pi^2 m_\chi^2}, & \text{Type 3 : } & \frac{c^4}{f_a^4} \frac{q^5}{16\pi^2 m_\chi}, \\ \text{Type 4 : } & \frac{c^4}{f_a^4} \frac{q^6}{16\pi^2 m_\chi^2}, & \text{Type 5 : } & \frac{c^4}{f_a^4} \frac{q^5}{16\pi^2 m_\chi}. \end{aligned} \quad (5.16)$$

This estimate suggests that contributions of these chiral loop diagrams are negligible compared to the perturbative loop-level contributions in section 5.1 and section 5.2. Therefore, we do not include them in our numerical analysis.

5.4 Higher-order ALP couplings

All loop contributions considered in this work involve four effective ALP couplings at mass dimension 5, such that the amplitude scales as c^4/f_a^4 . This raises the question if spin-independent scattering could also be generated by ALP couplings at higher orders in the ALP effective theory. In [73], an operator basis for all ALP couplings to SM particles up to mass dimension 8 has been constructed. With an intact shift symmetry, the only possible dimension-6 operator is a coupling of two ALPs to two Higgs fields. This coupling can indeed generate spin-independent scattering at loop level, with an amplitude scaling as c^2/f_a^2 . For a generic pseudo-scalar, this contribution has been studied in [18].

At mass dimension 7, all operators involve a single ALP field coupling to fermions through a partial derivative. This implies that no scalar interactions between fermion dark matter and quarks or gluons can be generated, because the ALP coupling to dark matter is momentum-suppressed.

With the exception of the ALP-Higgs contribution, we do not expect any other contributions to spin-independent dark matter-nucleon scattering of order $1/f_a^4$ or larger in the ALP effective theory.

⁹In the formal counting scheme of chPT, only the particles' momenta and the quark masses $m_q \sim \mathcal{O}(q^2/m_N)$ contribute to the power counting, while the potentially large low-energy constants are considered to be of $\mathcal{O}(1)$. Consequently, the vertex $NN\pi$ is formally of $\mathcal{O}(q)$, $NN\pi\pi$ and $\chi\chi NN$ are formally of $\mathcal{O}(q^2)$, while $\chi\chi\pi$ and $\chi\chi NN\pi$ are formally of $\mathcal{O}(q^3)$.

6 Numerical results

Equipped with the analytic results on ALP-mediated dark matter-nucleon scattering at tree level (section 4) and at one-loop level (section 5), we perform a numerical analysis of the various contributions of ALP-mediated scattering to the event rates expected in direct detection experiments. Throughout our analysis, we focus on Xenon-based experiments. The current experiments XENONnT [74], PandaX-4T [75] and DarkSide-50 [76] have world-leading sensitivity to dark matter-nucleon scattering for dark matter masses above a few GeV. The next-generation projects DARWIN/XLZD [77] and Pandax-xT [78] have the ambition to probe dark matter-nucleon scattering down to cross sections comparable with atmospheric neutrino scattering.

To quantify ALP-mediated dark matter scattering at these experiments, we calculate the event rate R from eq. (3.33) and the related non-relativistic nucleus and nucleon scattering cross sections, σ_{SI} and $\sigma_{\text{SI},N}$. The event rate R depends on the local dark matter velocity distribution $f_{\oplus}(\mathbf{v})$, for which we implement the ‘‘Standard Halo Model’’ from Ref. [56].

The non-relativistic scattering cross sections involve QCD form factors for nucleons and nuclei. For the scalar nucleon form factors, we use the central values and uncertainties presented in [47]. For the pseudo-scalar and CP-odd gluonic form factors, we neglect the uncertainties, as their contributions to the event rates are strongly suppressed compared to the scalar contributions. For the nucleus form factors, we use the Mathematica script published in [52].¹⁰ In our predictions, we take account of the relative abundances of various stable Xenon isotopes in the target material according to [80].

The hard scattering cross section is fully determined by the coupling and mass parameters of the ALP effective theory. Throughout our analysis, we set $f_a = 1 \text{ TeV}$, corresponding to a cutoff scale $\Lambda = 4\pi \text{ TeV}$. We express all results for non-relativistic scattering in terms of ALP couplings defined at this cutoff scale, using renormalization group evolution as described before. The ALP-dark matter coupling always enters the observables in combination with ALP couplings to SM particles. In our numerics, we therefore quote the product of ALP-SM and ALP-DM couplings, for instance $c_{uu}c_{\chi}$. For the ALP couplings to SM particles, we consider one coupling at a time, setting all other couplings to zero. This allows us to analyze the individual effects of these couplings on dark matter-nucleon scattering. We comment on potential effects of additional couplings wherever they would alter the predicted cross sections.

As all loop-induced dark matter interactions are UV-sensitive, they depend on the choice of renormalization scale. In certain regions of parameter space, this scale dependence can lead to substantial variations of the scattering cross section. In our predictions, we include

¹⁰We rescale the spin-dependent nuclear response functions $W_{\Sigma''}^{\tau\tau'}$ obtained from the script to agree with the shell-model calculation [55] in the long-wavelength limit. We do not include uncertainties on the nuclear response functions. The spin-independent response functions computed by several independent groups [52, 61, 79] agree up to percent level in the relevant energy recoil range.

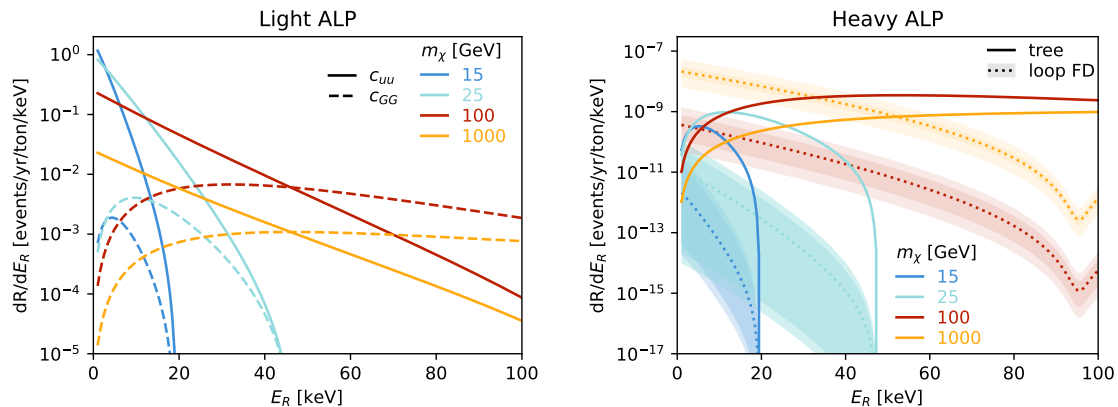


Figure 5: Energy recoil distribution dR/dE_R of Xenon nuclei due to dark matter scattering through flavor-diagonal ALP couplings; shown for ALP masses $m_a = 1$ MeV (left) and $m_a = 10$ GeV (right) and various dark matter masses, with $f_a = 1$ TeV. Left panel: spin-dependent tree-level scattering in two scenarios, $c_{uu}(\Lambda)c_\chi = 1$, $c_{qq \neq uu}(\Lambda) = c_{GG}(\Lambda) = 0$ (solid) and $c_{GG}(\Lambda)c_\chi = 1$, $c_{qq}(\Lambda) = 0$ (dashed). Right panel: spin-dependent tree-level (solid) and spin-independent one-loop (dotted) scattering for $c_{uu}(\Lambda)c_\chi = 1$, $c_{qq \neq uu}(\Lambda) = c_{GG}(\Lambda) = 0$. Colored bands indicate renormalization scale variation within $\mu \in [0.5, 2]m_a$ (darker shade) and nucleon form factor uncertainties (lighter shade).

renormalization scale variations in the range $[0.5, 2]\mu_R$, where μ_R is the central value chosen for the renormalization scale.

In what follows, we discuss the characteristics of the individual contributions to dark matter-nucleon scattering through ALPs with flavor-diagonal couplings (section 6.1) and flavor-changing couplings (section 6.2). In section 6.3, we finally make predictions for the total scattering rate at Xenon-based experiments and discuss how they can probe the parameter space of the ALP effective theory.

6.1 Flavor-diagonal ALP couplings

Flavor-diagonal ALP couplings to quarks generate spin-dependent dark matter-nucleus scattering at tree level and spin-independent scattering at one-loop level. In fig. 5, we show the energy recoil spectra of Xenon nuclei induced by elastic dark matter scattering. We distinguish between light ALPs with masses $m_a < \mu_{\text{chPT}}$, represented by the benchmark $m_a = 1$ MeV (left panel), and heavy ALPs with $m_a > \mu_{\text{chPT}}$, represented by $m_a = 10$ GeV (right panel).

For light ALPs, we show spin-dependent dark matter-nucleus scattering through tree-level ALP and pion exchange, based on the amplitude derived in section 4.2. The results are presented for two different scenarios with $c_{uu}(\Lambda)c_\chi = 1$ or $c_{GG}(\Lambda)c_\chi = 1$ and all respective other couplings set to zero at the cutoff scale Λ . The difference between the spectra in both scenarios can be explained analytically in the long-wavelength limit. In this limit, the differential cross section takes on the form of eq. (3.32), with the momentum-

dependent non-relativistic couplings from eq. (4.5). The energy spectrum exhibits zeros when $c_6^p S_p + c_6^n S_n = 0$ or, equivalently, when

$$E_R = \left[\frac{g_A}{g_0} \frac{\Delta c_{ud}}{c_{uu} + c_{dd} + 2c_{GG}} \frac{S_n - S_p}{S_n + S_p} - 1 \right] \frac{m_\pi^2}{2m_A}. \quad (6.1)$$

Here, all couplings are evaluated at μ_{chPT} . For $c_{GG}(\Lambda) = 1$, the solution (6.1) lies outside the physical region at $E_R \approx -2 \cdot 10^{-4}$ keV, manifesting itself as a decrease in the spectrum as $E_R \rightarrow 0$. The exact location of the cancellation point depends strongly on the momentum dependence of the form factor, as well as the values of the spin averages S_n and S_p , all of which are affected by large uncertainties. Regardless, as long as $|S_n| \gg |S_p|$, which is generally true for Xenon isotopes with odd neutron numbers, the decrease close to $E_R = 0$ should persist. For $c_{uu}(\Lambda) = 1$, the spectrum exhibits a zero for $E_R \approx 139$ keV. In this scenario, the energy spectrum is thus suppressed at large E_R , where it approaches the cancellation point. For light dark matter, the spectrum is cut off even earlier, as the maximum recoil energy is lower than for heavy dark matter.

For heavy ALPs, in fig. 5, right, we display spin-dependent dark matter-nucleus scattering through tree-level ALP exchange (section 4.1) and spin-independent scattering through loop-induced FD ALP couplings to quarks (section 5.1), both in the scenario $c_{uu}(\Lambda)c_\chi = 1$. Unlike in the case of light ALPs, here the scattering proceeds through a contact interaction. The energy recoil spectrum is therefore determined by the nuclear form factors. Accidental cancellations in the recoil spectrum could only occur for scenarios with tuned values of c_{qq} and c_{GG} , see eq. (4.3).

As anticipated, the predicted event rates in both cases are small. With light ALP mediators, the momentum suppression of spin-dependent scattering at tree level is partially lifted and the rate is a priori within the current reach of XENONnT. However, as discussed in section 2.2, searches for $K^+ \rightarrow \pi^+ X$ at NA62 [33] set strong bounds on c_{GG} and c_{qq} . In section 6.3, we will analyze the impact of these bounds on the predicted event rates.

With heavy ALPs, loop-induced spin-independent scattering through FD ALP couplings is similar in magnitude to spin-dependent scattering at tree level. At loop level, the momentum suppression is lifted, but this comes at the cost of a strong suppression by the cutoff scale of the ALP EFT, f_a^{-4} . This feature applies generically to ALP masses with $\mu_{\text{chPT}} < m_a \ll m_\chi$, for which the cross section has a mild, logarithmic dependence on ALP mass, see eq. (5.1). With couplings of $\mathcal{O}(1)$, the resulting event rates are far below the reach of current experiments and lie inside the neutrino fog. We will not consider them any further in our analysis.

6.2 Flavor-changing ALP couplings

Flavor-changing ALP couplings to quarks first contribute to dark matter-nucleus scattering at loop level, generating spin-independent interactions. The relevant scattering amplitude from eq. (5.6) probes the combination of ALP couplings $\bar{c}_{ut} c_\chi / f_a^2$, where we have defined

$$\bar{c}_{ut} = \sqrt{||c_{ut}^V|^2(\Lambda) - |c_{ut}^A|^2(\Lambda)|}. \quad (6.2)$$

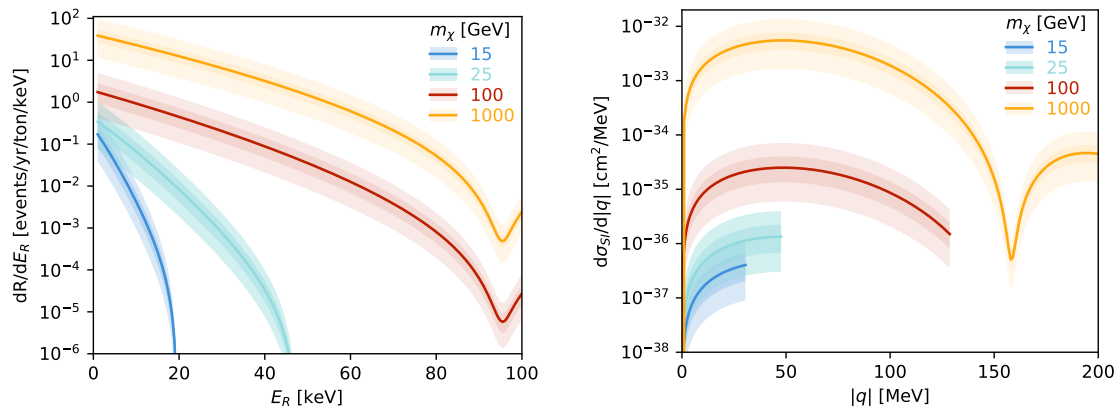


Figure 6: Energy recoil distribution dR/dE_R (left) and momentum exchange distribution $dR/d|q|$ (right) of Xenon nuclei due to dark-matter scattering through flavor-changing ALP couplings and various dark matter masses; shown for $m_a = 10$ GeV and fixed ALP couplings $\bar{c}_{ut}c_\chi/f_a^2 = 1/\text{TeV}^2$. The momentum distribution is shown for fixed dark matter velocity $v = 340$ km/s. Colored bands indicate renormalization scale variation within $\mu \in [0.5, 2]m_a$ (darker shade) and nucleon form factor uncertainties (lighter shade).

In fig. 6, we show the energy recoil distribution (left) and momentum exchange distribution for a fixed dark matter velocity of $v = 340$ km/s (right) for the heavy-ALP benchmark with $m_a = 10$ GeV. As for FD couplings, the shape of the spectra is determined by the nuclear form factors. In the right panel, the cutoff of the momentum distributions for light dark matter corresponds to the kinematic endpoint of momentum transfer in elastic scattering.

The recoil rate from spin-independent scattering through FC ALP couplings exceeds scattering through FD ALP couplings by 8 to 10 orders of magnitude, depending on the dark matter mass and recoil energy. As explained in section 5.2, this large enhancement is due to the relative overall scaling of the scattering cross section with the quark mass ratio $(m_t/m_u)^2 \approx 10^{10}$. Moreover, for $m_\chi \gg m_a, m_t$, the scattering rate through FC ALP couplings grows as $m_\chi^2 \ln^2(m_\chi^2/m_t^2)$. The sensitivity of direct detection experiments to this scenario is thus particularly high for heavy dark matter.

As we will see in section 6.3, the benchmark scenario from fig. 6 and a large part of the ALP EFT parameter space can be probed at current experiments, provided that the dark matter mass is sufficiently large. We stress again that the top-mass enhancement of scattering through FC couplings requires ALP couplings to both left- and right-handed quarks to be present. Additional FD ALP couplings have little effect on these results, as the corresponding scattering amplitudes do not feature such an enhancement.

6.3 Predictions for Xenon-based experiments

By integrating the recoil spectra from the previous sections over the recoil energy, we obtain predictions for the expected event rates at Xenon-based direct detection experiments. In fig. 7, we show these event rates for spin-dependent scattering through light

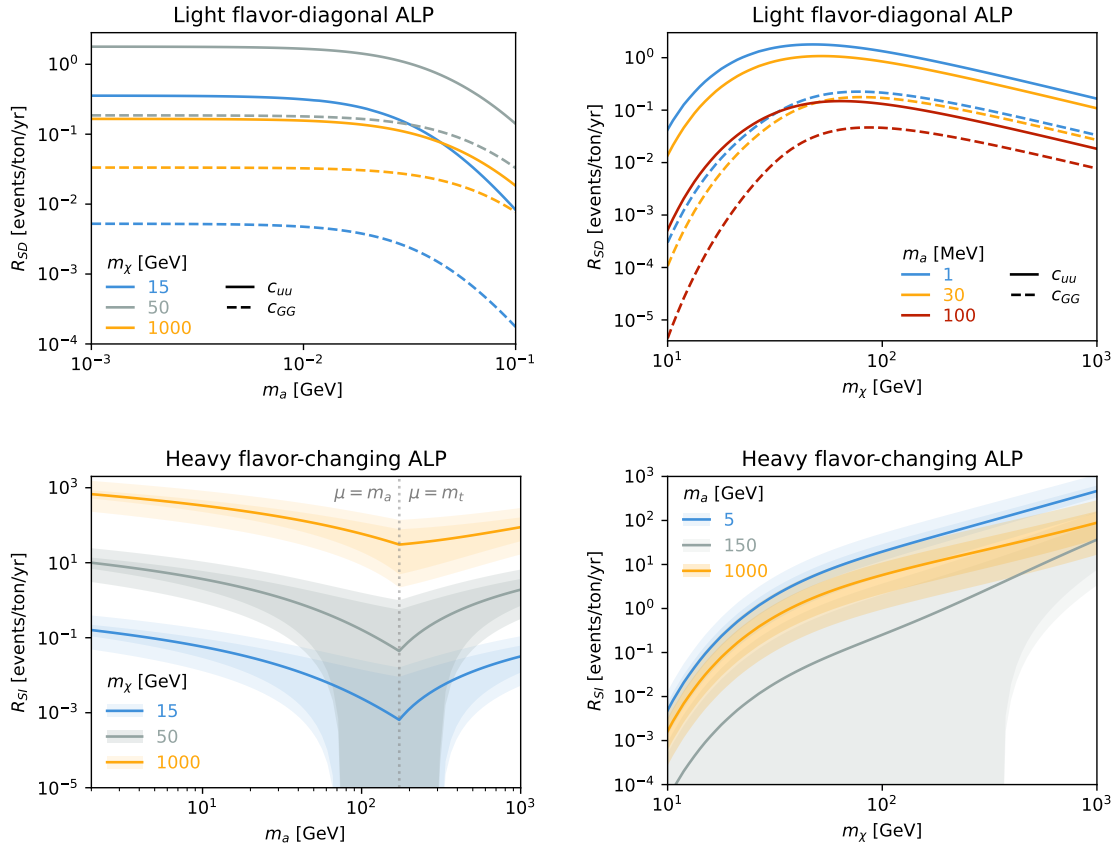


Figure 7: Total predicted event rate R at the XENONnT experiment per ton-year. The detector efficiency and accessible energy recoil range described in [81] are taken into account. Upper row: spin-dependent scattering of light ALPs in two scenarios, $c_{uu}c_\chi/f_a^2 = 1/\text{TeV}^2$ (solid) and $c_{GG}c_\chi/f_a^2 = 1/\text{TeV}^2$ (dashed). Lower row: spin-independent scattering of heavy ALPs with flavor-changing couplings for $\bar{c}_{ut}c_\chi/f_a^2 = 1/\text{TeV}^2$. Colored bands indicate renormalization scale variation within $\mu \in [0.5, 2]m_a$ (darker shade) and nucleon form factor uncertainties (lighter shade).

ALPs with flavor-diagonal couplings (top row) and for spin-independent scattering through heavy ALPs with flavor-changing couplings (bottom row).

For ALPs with masses $m_a \lesssim 20$ MeV and FD couplings, the predicted event rates for spin-dependent scattering approach the constant limit of an effectively massless ALP, see fig. 7 top left. In this region, the maximum event rates range around a few events per ton per year for ALP couplings $c_{uu}c_\chi/f_a^2 = 1/\text{TeV}^2$. However, the strong constraints from NA62’s $K^+ \rightarrow \pi^+ X$ search on the ALP-quark coupling (2.18) and ALP-gluon coupling (2.15) suppress the rate by about 4-5 orders of magnitude. This is far beyond the reach of current and future direct detection experiments. For ALPs above the kaon mass, bounds on the couplings are much looser. However, for $m_a \gtrsim 20$ MeV the scattering rate drops quickly because the $1/q^2$ enhancement of the ALP propagator at small momenta is cut off by

the ALP mass. An observation of dark matter-nucleon scattering through a light ALP at Xenon-based experiments is therefore extremely unlikely to occur.

On the contrary, the prospects to probe spin-independent scattering through ALPs with FC couplings are very promising. In the bottom panels of fig. 7, we predict scattering rates of up to 1000 per ton-year for $m_\chi = 1$ TeV. The growth of the scattering amplitude with the dark matter mass over-compensates the drop in the number density, such that the sensitivity is maximized for heavy dark matter. The ALP mass dependence is comparatively moderate. In fig. 7, bottom left, the kink at $m_a = m_t$ is due to the change in renormalization scale. For $m_a < m_t$, one would first integrate out the top and choose the ALP mass as renormalization scale, and vice versa. The large scale dependence in this mass region is due to an accidental cancellation of the loop function for certain values of the mass parameters and renormalization scale. The strong renormalization scale dependence is an artifact of the UV sensitivity of the loop function, which originates from the missing heavy degrees of freedom in the ALP effective theory.

To compare the predicted scattering rates against data, we calculate the average cross section for spin-independent dark matter-nucleon scattering from eq. (3.31), $\sigma_{SI,N}$, which is reported by the experimental collaborations. In fig. 8, we show this cross section for two ALP mass benchmarks and fixed FC coupling $\bar{c}_{ut}c_\chi/f_a^2 = 1/\text{TeV}^2$. From the figure, it is apparent that XENONnT is already sensitive to these benchmarks for dark matter with masses $m_\chi \gtrsim 30$ GeV. For light dark matter with $m_\chi \lesssim 10$ GeV, the predicted cross section lies below the boundary of the neutrino fog and orders of magnitude below the sensitivity of current experiments. In this mass region, it will thus be very unlikely to observe ALP-mediated scattering at Xenon-based experiments.

To quantify how much of the ALP parameter space can be probed with dark matter-nucleon scattering, in fig. 9 we show the current 90% C.L. upper bounds on the product of ALP couplings, $\bar{c}_{ut}c_\chi$, at direct detection experiments. As anticipated, the sensitivity is particularly high at large dark matter masses. A direct comparison with collider searches is limited for two reasons. First, dark matter scattering relies on the product $\bar{c}_{ut}c_\chi$, while colliders probe the ALP-quark coupling independently from the dark matter coupling. Second, dark matter scattering involves the combination $\bar{c}_{ut}^2 \propto (\mathbf{c}_u)_{13}(\mathbf{c}_U)_{13}$ from eq. (6.2), while the LHC bound $|(\mathbf{c}_u)_{13}|/f_a \lesssim 0.1/\text{TeV}$ from eq. (2.30) applies only if $(\mathbf{c}_u)_{13} \gg (\mathbf{c}_U)_{13}$. We therefore do not attempt a comparison with collider searches, which would only apply for a restricted part of the ALP parameter space.

For heavy ALPs with sizeable couplings to left-handed quarks, direct detection experiments currently offer the best sensitivity to the FC coupling \bar{c}_{ut} – provided that the ALP also couples to the dark sector. As discussed in section 2.3, dedicated searches for top-associated ALP production with prompt hadronic decays, for instance through $pp \rightarrow tja$, $a \rightarrow jbj$ with a bottom-quark jet j_b , would be required to probe this scenario at the LHC.

To estimate the reach of future direct detection experiments, we also show the ALP couplings corresponding to a cross section at the boundary of the neutrino fog. The anticipated

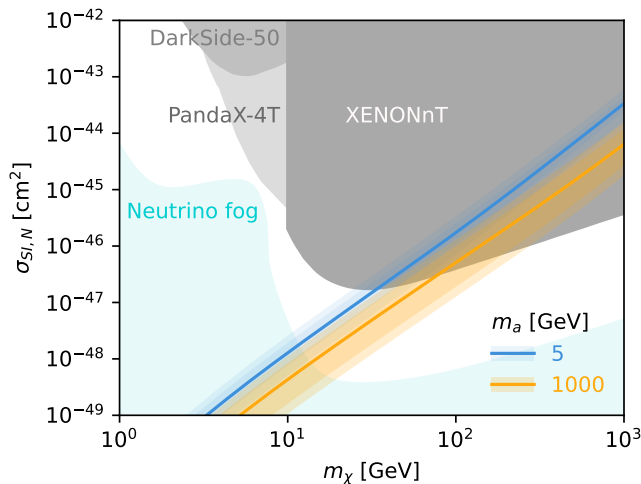


Figure 8: Cross section for spin-independent dark matter-nucleon scattering, $\sigma_{SI,N}$, versus dark matter mass, shown for different ALP masses and fixed couplings $\bar{c}_{ut}c_\chi/f_a^2 = 1/\text{TeV}^2$. Grey areas: experimental bounds from XENONnT [81], PandaX-4T [82] and DarkSide-50 [76]. Blue area: neutrino fog [83]. Colored bands indicate renormalization scale variation within $\mu \in [0.5, 2]m_a$ (darker shade) and nucleon form factor uncertainties (lighter shade).

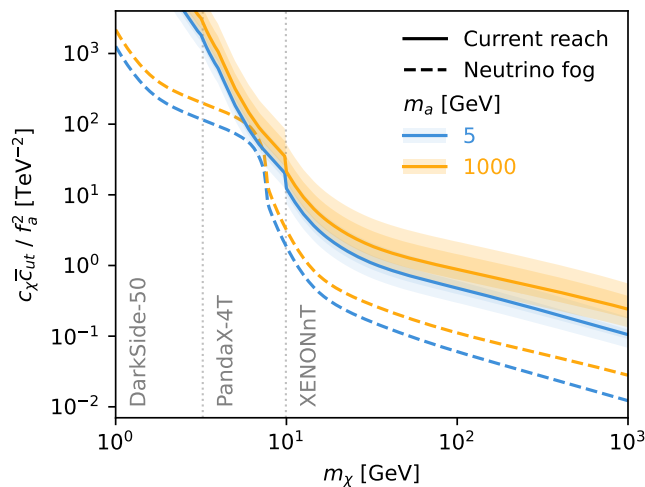


Figure 9: 90% C.L. upper bounds on the combination of ALP couplings probed by dark matter-nucleon scattering, $\bar{c}_{ut}c_\chi/f_a^2$, versus dark matter mass, for different ALP masses. Solid lines: current upper bounds from XENONnT [81], PandaX-4T [82], and DarkSide-50 [76]. Dashed lines: projected bounds corresponding to cross sections at the neutrino fog boundary [83]. Colored bands indicate renormalization scale variation within $\mu \in [0.5, 2]m_a$ (darker shade) and nucleon form factor uncertainties (lighter shade).

sensitivity to the effective couplings increases by an order of magnitude. In the framework of the ALP effective theory, this means that dark matter-nucleon scattering will probe new physics beyond the TeV scale, provided that it generates sizeable flavor-changing couplings to ALPs. This is a remarkable result, given that the underlying scattering amplitude is generated at the loop level and the scattering occurs at very low energy scales, with a four-fold suppression by the cutoff scale $\Lambda \propto f_a$.

Let us close with a remark on light ALPs with masses $m_a < \mu_{\text{chPT}}$ and FC couplings. While such a scenario requires a dedicated calculation in chiral perturbation theory, we expect a priori sizeable scattering rates also in this case. This is suggested by the logarithmic growth of the event rate for small m_a , see the bottom left panel of fig. 7. At colliders, this mass region is probed by the total B meson width, as well as searches for invisible ALPs in $B \rightarrow K\nu\bar{\nu}$ and $K \rightarrow \pi X$, as discussed in section 2.3. Taken together, these observables constrain FC ALP couplings to $|c_{ut}^V - c_{ut}^A|/f_a < (0.004 \dots 5 \cdot 10^{-8})/\text{TeV}$, depending on the ALP mass. These strong bounds make an observation at direct detection experiments very challenging, even for heavy dark matter where the scattering rate is maximized.

7 Conclusion

With this systematic analysis of ALP-mediated dark matter-nucleon scattering, we have identified several qualitatively different contributions to spin-dependent and spin-independent scattering. Spin-dependent scattering is generated at tree level through ALP exchange, but momentum-suppressed. A priori, this suppression can be lifted if the ALP is lighter than the typical momentum transfer. However, strong bounds on the ALP couplings to quarks and gluons from searches for invisible ALPs produced in kaon decays at NA62 suppress the predicted scattering rates far below the reach of current and future direct detection experiments.

Spin-independent scattering is generated through two kinds of loop processes. At energies above the scale of chiral symmetry breaking in QCD, double ALP exchange generates scalar interactions between dark matter and the quarks and gluons inside the nucleon. With flavor-diagonal ALP couplings, the scattering amplitude is suppressed as c^4/f_a^4 , which leads to negligible event rates for experimental purposes. At low energies, loop exchange of virtual mesons and nucleons generates scalar interactions in chiral perturbation theory. However, these contributions are suppressed by several powers of the small momentum transfer, in addition to the c^4/f_a^4 suppression.

The phenomenology of ALP-mediated dark matter scattering completely changes if the ALP has flavor-changing couplings to top and up quarks. The large top mass enhances the loop-induced scattering amplitude by 5 orders of magnitude compared to contributions from ALPs with flavor-diagonal couplings, compensating for the loop and cutoff-scale suppression. Spin-independent dark matter-nucleon scattering through flavor-changing ALPs occurs at high rates, which are already probed by current Xenon-based experiments. The scattering cross section grows with the dark matter mass, so that event rates are highest

for heavy dark matter, despite the comparatively lower number density. Model-dependent contributions from particles living above the cutoff scale of the ALP effective theory could further enhance the scattering rate.

The future direct detection experiments DARWIN/XLZD and PandaX-xT are expected to probe large parts of the ALP parameter space through spin-independent scattering. Our predictions suggest that their sensitivity to flavor-changing ALP couplings will exceed that of collider searches, provided that the ALP has sizeable couplings to dark matter. We encourage the experimental collaborations to consider ALP-mediated dark matter as an interesting target for their searches.

A Loop functions for spin-independent scattering

In this appendix, we provide the relativistic one-loop amplitudes for ALP-mediated dark matter-nucleon scattering. These results are valid for on-shell external states with arbitrary momentum and apply for any ALP mass above the scale of chiral symmetry breaking, $m_a > \mu_{\text{chPT}}$.

Flavor-diagonal ALP couplings For FD ALP-quark couplings, the one-loop amplitude for the scattering process $\chi(p) + q(k) \rightarrow \chi(p') + q(k')$ with momentum exchange $q = k' - k$ is

$$\begin{aligned} \mathcal{M}_{\text{loop}}^{\text{FD}} = \frac{m_q m_\chi c_{qq}^2 c_\chi^2}{16\pi^2 f_a^4} & \left\{ -m_\chi (\bar{u}_\chi \gamma^\mu u_\chi) (\bar{u}_q u_q) C_\mu(q, p, m_a, m_a, m_\chi) \right. \\ & + m_q (\bar{u}_\chi u_\chi) (\bar{u}_q \gamma^\mu u_q) C_\mu(-k, q, m_a, m_q, m_a) + \frac{1}{2} (\bar{u}_\chi u_\chi) (\bar{u}_q u_q) B_0(q, m_a, m_a) \\ & - m_\chi m_q (\bar{u}_\chi \gamma^\mu u_\chi) (\bar{u}_q \gamma^\nu u_q) \left[D_{\mu\nu}(-k, q, p, m_a, m_q, m_a, m_\chi) \right. \\ & \left. \left. - D_{\mu\nu}(k', q, p, m_a, m_q, m_a, m_\chi) \right] \right\}, \end{aligned} \quad (\text{A.1})$$

where we have used the shorthand notations

$$\bar{u}_\chi \equiv \bar{u}_\chi(p'), \quad u_\chi \equiv u_\chi(p), \quad \bar{u}_q \equiv \bar{u}_q(k'), \quad u_q \equiv u_q(k). \quad (\text{A.2})$$

The corresponding Feynman diagram is given in fig. 3, left. The scalar and tensor integral functions B_0 , C_μ and $D_{\mu\nu}$ are defined as in [84]. Effective scalar interactions $(\bar{u}_\chi u_\chi)(\bar{u}_q u_q)$ are generated by the B_0 and C_μ terms. Effective vector interactions $(\bar{u}_\chi \gamma^\mu u_\chi)(\bar{u}_q \gamma_\mu u_q)$ are due to the $D_{\mu\nu}$ terms. They are suppressed by at least a factor of $\mathcal{O}(m_q/m_a)$ compared to the scalar interactions.

Our result in (A.1) differs from that obtained in [18, 19]. The latter articles consider a generic pseudo-scalar mediator P with a coupling $\bar{\psi} i \gamma_5 \psi P$ to fermions ψ . In our case the pseudo-scalar ALP has derivative couplings to fermions, see eq. (2.1), which makes a difference in the loop function. However, we are puzzled by the fact that the loop functions in [18] and [19] seem to disagree.

Flavor-changing ALP couplings For FC ALP-top-up couplings, the one-loop scattering amplitude for $\chi(p) + u(k) \rightarrow \chi(p') + u(k')$ is

$$\begin{aligned} \mathcal{M}_{\text{loop}}^{\text{FC}} = & -\frac{m_t m_\chi c_\chi^2}{64\pi^2 f_a^4} \left\{ (\bar{u}_\chi u_\chi) (\bar{u}_u \mathcal{C}_{ut}^- u_u) [B_0(q, m_a, m_a) + m_t^2 C_0(k, -q, m_a, m_t, m_a)] \right. \\ & + m_\chi (\bar{u}_\chi \gamma^\mu u_\chi) (\bar{u}_u \mathcal{C}_{ut}^- u_u) [-2C_\mu(q, p, m_a, m_a, m_\chi) \\ & + m_t^2 D_\mu(k, -q, -p, m_a, m_t, m_a, m_\chi) + m_t^2 D_\mu(-k', -q, -p, m_a, m_t, m_a, m_\chi)] \\ & + m_\chi m_t (\bar{u}_\chi \gamma^\mu u_\chi) (\bar{u}_u \gamma^\nu \mathcal{C}_{ut}^+ u_u) [D_{\mu\nu}(k, -q, -p, m_a, m_t, m_a, m_\chi) \\ & \left. - D_{\mu\nu}(-k', -q, -p, m_a, m_t, m_a, m_\chi)] + \mathcal{O}\left(\frac{m_u}{m_t}\right) \right\}, \quad (\text{A.3}) \end{aligned}$$

which depends on the ALP-quark couplings through the combinations

$$\begin{aligned} \mathcal{C}_{ut}^- &= |c_{ut}^V|^2 - |c_{ut}^A|^2 + 2i \text{Im}[c_{ut}^V (c_{ut}^A)^*] \gamma^5, \\ \mathcal{C}_{ut}^+ &= |c_{ut}^V|^2 + |c_{ut}^A|^2 + 2 \text{Re}[c_{ut}^V (c_{ut}^A)^*] \gamma^5. \end{aligned} \quad (\text{A.4})$$

The corresponding Feynman diagram is given in fig. 3, right. As in the FD case, contributions from $D_{\mu\nu}$ are suppressed, in this case by $|\mathbf{k}^{(\prime)}|/m_t$.

References

- [1] M. Schumann, *Direct Detection of WIMP Dark Matter: Concepts and Status*, *J. Phys. G* **46** (2019), no. 10 103003, [[1903.03026](#)].
- [2] J. Billard et al., *Direct detection of dark matter—APPEC committee report**, *Rept. Prog. Phys.* **85** (2022), no. 5 056201, [[2104.07634](#)].
- [3] D. S. Akerib et al., *Snowmass2021 Cosmic Frontier Dark Matter Direct Detection to the Neutrino Fog*, in *Snowmass 2021*, 3, 2022. [2203.08084](#).
- [4] M. Cirelli, A. Strumia, and J. Zupan, *Dark Matter*, [2406.01705](#).
- [5] G. Arcadi, D. Cabo-Almeida, M. Dutra, P. Ghosh, M. Lindner, et al., *The Waning of the WIMP: Endgame?*, *Eur. Phys. J. C* **85** (2025), no. 2 152, [[2403.15860](#)].
- [6] N. Bernal, M. Heikinheimo, T. Tenkanen, K. Tuominen, and V. Vaskonen, *The Dawn of FIMP Dark Matter: A Review of Models and Constraints*, *Int. J. Mod. Phys. A* **32** (2017), no. 27 1730023, [[1706.07442](#)].
- [7] M. W. Goodman and E. Witten, *Detectability of Certain Dark Matter Candidates*, *Phys. Rev. D* **31** (1985) 3059.
- [8] P. Agrawal, Z. Chacko, C. Kilic, and R. K. Mishra, *A Classification of Dark Matter Candidates with Primarily Spin-Dependent Interactions with Matter*, [1003.1912](#).
- [9] M. Pospelov, A. Ritz, and M. B. Voloshin, *Secluded WIMP Dark Matter*, *Phys. Lett. B* **662** (2008) 53–61, [[0711.4866](#)].
- [10] J. Jaeckel and A. Ringwald, *The Low-Energy Frontier of Particle Physics*, *Ann. Rev. Nucl. Part. Sci.* **60** (2010) 405–437, [[1002.0329](#)].
- [11] X. Chu, T. Hambye, and M. H. G. Tytgat, *The Four Basic Ways of Creating Dark Matter Through a Portal*, *JCAP* **05** (2012) 034, [[1112.0493](#)].

- [12] A. Djouadi, A. Falkowski, Y. Mambrini, and J. Quevillon, *Direct Detection of Higgs-Portal Dark Matter at the LHC*, *Eur. Phys. J. C* **73** (2013), no. 6 2455, [[1205.3169](#)].
- [13] A. Freitas, S. Westhoff, and J. Zupan, *Integrating in the Higgs Portal to Fermion Dark Matter*, *JHEP* **09** (2015) 015, [[1506.04149](#)].
- [14] G. Arcadi, A. Djouadi, and M. Raidal, *Dark Matter through the Higgs portal*, *Phys. Rept.* **842** (2020) 1–180, [[1903.03616](#)].
- [15] R. Essig, J. Mardon, and T. Volansky, *Direct Detection of Sub-GeV Dark Matter*, *Phys. Rev. D* **85** (2012) 076007, [[1108.5383](#)].
- [16] M. Fabbrichesi, E. Gabrielli, and G. Lanfranchi, *The Dark Photon*, [2005.01515](#).
- [17] M. Freytsis and Z. Ligeti, *On dark matter models with uniquely spin-dependent detection possibilities*, *Phys. Rev. D* **83** (2011) 115009, [[1012.5317](#)].
- [18] S. Ipek, D. McKeen, and A. E. Nelson, *A Renormalizable Model for the Galactic Center Gamma Ray Excess from Dark Matter Annihilation*, *Phys. Rev. D* **90** (2014), no. 5 055021, [[1404.3716](#)].
- [19] G. Arcadi, M. Lindner, F. S. Queiroz, W. Rodejohann, and S. Vogl, *Pseudoscalar Mediators: A WIMP model at the Neutrino Floor*, *JCAP* **03** (2018) 042, [[1711.02110](#)].
- [20] D. Buttazzo, P. Panci, D. Teresi, and R. Ziegler, *Xenon1T excess from electron recoils of non-relativistic Dark Matter*, *Phys. Lett. B* **817** (2021) 136310, [[2011.08919](#)].
- [21] H. Georgi, D. B. Kaplan, and L. Randall, *Manifesting the Invisible Axion at Low-energies*, *Phys. Lett. B* **169** (1986) 73–78.
- [22] P. J. Fitzpatrick, Y. Hochberg, E. Kuflik, R. Ovadia, and Y. Soreq, *Dark matter through the axion-gluon portal*, *Phys. Rev. D* **108** (2023), no. 7 075003, [[2306.03128](#)].
- [23] G. Armando, P. Panci, J. Weiss, and R. Ziegler, *Leptonic ALP portal to the dark sector*, *Phys. Rev. D* **109** (2024), no. 5 055029, [[2310.05827](#)].
- [24] J. A. Dror, S. Gori, and P. Munbodh, *QCD axion-mediated dark matter*, *JHEP* **09** (2023) 128, [[2306.03145](#)].
- [25] G. G. Raffelt, *Astrophysical axion bounds*, *Lect. Notes Phys.* **741** (2008) 51–71, [[hep-ph/0611350](#)].
- [26] P. F. Depta, M. Hufnagel, and K. Schmidt-Hoberg, *Robust cosmological constraints on axion-like particles*, *JCAP* **05** (2020) 009, [[2002.08370](#)].
- [27] A. Caputo and G. Raffelt, *Astrophysical Axion Bounds: The 2024 Edition*, *PoS COSMICWISPerS* (2024) 041, [[2401.13728](#)].
- [28] M. Bauer, M. Neubert, S. Renner, M. Schnubel, and A. Thamm, *The Low-Energy Effective Theory of Axions and ALPs*, *JHEP* **04** (2021) 063, [[2012.12272](#)].
- [29] M. Bauer, M. Neubert, and A. Thamm, *Collider Probes of Axion-Like Particles*, *JHEP* **12** (2017) 044, [[1708.00443](#)].
- [30] M. Bauer, M. Neubert, S. Renner, M. Schnubel, and A. Thamm, *Flavor probes of axion-like particles*, *JHEP* **09** (2022) 056, [[2110.10698](#)].
- [31] T. Ferber, A. Filimonova, R. Schäfer, and S. Westhoff, *Displaced or invisible? ALPs from B decays at Belle II*, *JHEP* **04** (2023) 131, [[2201.06580](#)].

- [32] N. Gubernari, A. Kokulu, and D. van Dyk, *$B \rightarrow P$ and $B \rightarrow V$ Form Factors from B -Meson Light-Cone Sum Rules beyond Leading Twist*, *JHEP* **01** (2019) 150, [[1811.00983](#)].
- [33] **NA62**, E. Cortina Gil et al., *Searches for hidden sectors using $K^+ \rightarrow \pi^+ X$ decays*, [2507.17286](#).
- [34] **NA62**, E. Cortina Gil et al., *Search for π^0 decays to invisible particles*, *JHEP* **02** (2021) 201, [[2010.07644](#)].
- [35] M. Abumusabh, G. Dujany, D. Guadagnoli, A. Iohner, and C. Toni, *The $B^+ \rightarrow K^+ \nu \bar{\nu}$ decay as a search for the QCD axion*, [2510.18953](#).
- [36] **BaBar**, J. P. Lees et al., *Search for an Axionlike Particle in B Meson Decays*, *Phys. Rev. Lett.* **128** (2022), no. 13 131802, [[2111.01800](#)].
- [37] M. B. Gavela, J. M. No, V. Sanz, and J. F. de Trocóniz, *Nonresonant Searches for Axionlike Particles at the LHC*, *Phys. Rev. Lett.* **124** (2020), no. 5 051802, [[1905.12953](#)].
- [38] S. Bruggisser, L. Grabitz, and S. Westhoff, *Global analysis of the ALP effective theory*, *JHEP* **01** (2024) 092, [[2308.11703](#)].
- [39] J. Martin Camalich, M. Pospelov, P. N. H. Vuong, R. Ziegler, and J. Zupan, *Quark Flavor Phenomenology of the QCD Axion*, *Phys. Rev. D* **102** (2020), no. 1 015023, [[2002.04623](#)].
- [40] F. Bishara, J. Brod, B. Grinstein, and J. Zupan, *Chiral Effective Theory of Dark Matter Direct Detection*, *JCAP* **02** (2017) 009, [[1611.00368](#)].
- [41] A. Carmona, F. Elahi, C. Scherb, and P. Schwaller, *The ALPs from the top: searching for long lived axion-like particles from exotic top decays*, *JHEP* **07** (2022) 122, [[2202.09371](#)].
- [42] K. Cheung, F.-T. Chung, G. Cottin, and Z. S. Wang, *Quark flavor violation and axion-like particles from top-quark decays at the LHC*, *JHEP* **07** (2024) 209, [[2404.06126](#)].
- [43] A. V. Phan and S. Westhoff, *Precise tests of the axion coupling to tops*, *JHEP* **05** (2024) 075, [[2312.00872](#)].
- [44] S. Blasi, F. Maltoni, A. Mariotti, K. Mimasu, D. Pagani, et al., *Top-philic ALP phenomenology at the LHC: the elusive mass-window*, *JHEP* **06** (2024) 077, [[2311.16048](#)].
- [45] **Fermilab Lattice, MILC**, J. A. Bailey et al., *$|V_{ub}|$ from $B \rightarrow \pi \ell \nu$ decays and $(2+1)$ -flavor lattice QCD*, *Phys. Rev. D* **92** (2015), no. 1 014024, [[1503.07839](#)].
- [46] **Particle Data Group**, S. Navas et al., *Review of particle physics*, *Phys. Rev. D* **110** (2024), no. 3 030001.
- [47] F. Bishara, J. Brod, B. Grinstein, and J. Zupan, *From quarks to nucleons in dark matter direct detection*, *JHEP* **11** (2017) 059, [[1707.06998](#)].
- [48] J. Brod, A. Gootjes-Dreesbach, M. Tamaro, and J. Zupan, *Effective Field Theory for Dark Matter Direct Detection up to Dimension Seven*, *JHEP* **10** (2018) 065, [[1710.10218](#)].
[Erratum: *JHEP* 07, 012 (2023)].
- [49] R. J. Hill and M. P. Solon, *Standard Model anatomy of WIMP dark matter direct detection II: QCD analysis and hadronic matrix elements*, *Phys. Rev. D* **91** (2015) 043505, [[1409.8290](#)].
- [50] J. Gasser, M. E. Sainio, and A. Svarc, *Nucleons with chiral loops*, *Nucl. Phys. B* **307** (1988) 779–853.

- [51] J. Liang, Y.-B. Yang, T. Draper, M. Gong, and K.-F. Liu, *Quark spins and Anomalous Ward Identity*, *Phys. Rev. D* **98** (2018), no. 7 074505, [[1806.08366](#)].
- [52] N. Anand, A. L. Fitzpatrick, and W. C. Haxton, *Weakly interacting massive particle-nucleus elastic scattering response*, *Phys. Rev. C* **89** (2014), no. 6 065501, [[1308.6288](#)].
- [53] A. L. Fitzpatrick, W. Haxton, E. Katz, N. Lubbers, and Y. Xu, *The Effective Field Theory of Dark Matter Direct Detection*, *JCAP* **02** (2013) 004, [[1203.3542](#)].
- [54] R. H. Helm, *Inelastic and Elastic Scattering of 187-Mev Electrons from Selected Even-Even Nuclei*, *Phys. Rev.* **104** (1956) 1466–1475.
- [55] P. Klos, J. Menéndez, D. Gazit, and A. Schwenk, *Large-scale nuclear structure calculations for spin-dependent WIMP scattering with chiral effective field theory currents*, *Phys. Rev. D* **88** (2013), no. 8 083516, [[1304.7684](#)]. [Erratum: *Phys.Rev.D* 89, 029901 (2014)].
- [56] D. Baxter et al., *Recommended conventions for reporting results from direct dark matter searches*, *Eur. Phys. J. C* **81** (2021), no. 10 907, [[2105.00599](#)].
- [57] K. J. Bae and J. Kim, *Axion-Mediated Inelastic Dark Matter*, [2312.11210](#).
- [58] L. Di Luzio, R. Gröber, and P. Paradisi, *Hunting for CP-violating axionlike particle interactions*, *Phys. Rev. D* **104** (2021), no. 9 095027, [[2010.13760](#)].
- [59] R. J. Hill and M. P. Solon, *Universal behavior in the scattering of heavy, weakly interacting dark matter on nuclear targets*, *Phys. Lett. B* **707** (2012) 539–545, [[1111.0016](#)].
- [60] R. J. Hill and M. P. Solon, *WIMP-nucleon scattering with heavy WIMP effective theory*, *Phys. Rev. Lett.* **112** (2014) 211602, [[1309.4092](#)].
- [61] M. Hoferichter, P. Klos, J. Menéndez, and A. Schwenk, *Analysis strategies for general spin-independent WIMP-nucleus scattering*, *Phys. Rev. D* **94** (2016), no. 6 063505, [[1605.08043](#)].
- [62] H. Georgi, *An Effective Field Theory for Heavy Quarks at Low-energies*, *Phys. Lett. B* **240** (1990) 447–450.
- [63] M. Neubert, *Heavy quark symmetry*, *Phys. Rept.* **245** (1994) 259–396, [[hep-ph/9306320](#)].
- [64] E. E. Jenkins and A. V. Manohar, *Baryon chiral perturbation theory using a heavy fermion Lagrangian*, *Phys. Lett. B* **255** (1991) 558–562.
- [65] A. F. Falk, H. Georgi, B. Grinstein, and M. B. Wise, *Heavy Meson Form-factors From QCD*, *Nucl. Phys. B* **343** (1990) 1–13.
- [66] T. Mannel, W. Roberts, and Z. Ryzak, *A Derivation of the heavy quark effective Lagrangian from QCD*, *Nucl. Phys. B* **368** (1992) 204–217.
- [67] V. Bernard, N. Kaiser, and U.-G. Meissner, *Chiral dynamics in nucleons and nuclei*, *Int. J. Mod. Phys. E* **4** (1995) 193–346, [[hep-ph/9501384](#)].
- [68] A. Crivellin, M. Hoferichter, and M. Procura, *Accurate evaluation of hadronic uncertainties in spin-independent WIMP-nucleon scattering: Disentangling two- and three-flavor effects*, *Phys. Rev. D* **89** (2014) 054021, [[1312.4951](#)].
- [69] G. Grilli di Cortona, E. Hardy, J. Pardo Vega, and G. Villadoro, *The QCD axion, precisely*, *JHEP* **01** (2016) 034, [[1511.02867](#)].
- [70] S. Weinberg, *Nuclear forces from chiral Lagrangians*, *Phys. Lett. B* **251** (1990) 288–292.

- [71] E. Epelbaum, H. Krebs, and U. G. Meißner, *Improved chiral nucleon-nucleon potential up to next-to-next-to-next-to-leading order*, *Eur. Phys. J. A* **51** (2015), no. 5 53, [[1412.0142](#)].
- [72] C. Körber, A. Nogga, and J. de Vries, *First-principle calculations of Dark Matter scattering off light nuclei*, *Phys. Rev. C* **96** (2017), no. 3 035805, [[1704.01150](#)].
- [73] C. Grojean, J. Kley, and C.-Y. Yao, *Hilbert series for ALP EFTs*, *JHEP* **11** (2023) 196, [[2307.08563](#)].
- [74] **XENON**, E. Aprile et al., *First Dark Matter Search with Nuclear Recoils from the XENONnT Experiment*, *Phys. Rev. Lett.* **131** (2023), no. 4 041003, [[2303.14729](#)].
- [75] **PandaX-4T**, Y. Meng et al., *Dark Matter Search Results from the PandaX-4T Commissioning Run*, *Phys. Rev. Lett.* **127** (2021), no. 26 261802, [[2107.13438](#)].
- [76] **DarkSide**, P. Agnes et al., *Search for Dark-Matter–Nucleon Interactions via Migdal Effect with DarkSide-50*, *Phys. Rev. Lett.* **130** (2023), no. 10 101001, [[2207.11967](#)].
- [77] J. Aalbers et al., *A next-generation liquid xenon observatory for dark matter and neutrino physics*, *J. Phys. G* **50** (2023), no. 1 013001, [[2203.02309](#)].
- [78] **PANDA-X**, **PandaX**, A. Abdukerim et al., *PandaX-xT—A deep underground multi-ten-tonne liquid xenon observatory*, *Sci. China Phys. Mech. Astron.* **68** (2025), no. 2 221011, [[2402.03596](#)].
- [79] L. Vietze, P. Klos, J. Menéndez, W. C. Haxton, and A. Schwenk, *Nuclear structure aspects of spin-independent WIMP scattering off xenon*, *Phys. Rev. D* **91** (2015), no. 4 043520, [[1412.6091](#)].
- [80] F. G. Kondev, M. Wang, W. J. Huang, S. Naimi, and G. Audi, *The NUBASE2020 evaluation of nuclear physics properties*, *Chin. Phys. C* **45** (2021), no. 3 030001.
- [81] **XENON**, E. Aprile et al., *WIMP Dark Matter Search using a 3.1 tonne \times year Exposure of the XENONnT Experiment*, [2502.18005](#).
- [82] **PandaX**, D. Huang et al., *Search for Dark-Matter–Nucleon Interactions with a Dark Mediator in PandaX-4T*, *Phys. Rev. Lett.* **131** (2023), no. 19 191002, [[2308.01540](#)].
- [83] C. A. J. O’Hare, *New Definition of the Neutrino Floor for Direct Dark Matter Searches*, *Phys. Rev. Lett.* **127** (2021), no. 25 251802, [[2109.03116](#)].
- [84] A. Denner, *Techniques for calculation of electroweak radiative corrections at the one loop level and results for W physics at LEP-200*, *Fortsch. Phys.* **41** (1993) 307–420, [[0709.1075](#)].